Journal Name

ARTICLE

Controlling the Emission Efficiency of Blue-Green Iridium(III) Phosphorescent Emitters and Applications in Solution-Processed Organic Light-Emitting Diodes

Received 00th January 20xx,
Accepted 00th January 20xx

DOI: 10.1039/x0xx00000x

www.rsc.org/

Muhammad T. Sajjad,[a] Nidhi Sharma,[a,b] Amlan K. Pal,[b] Kamrul Hasan,[c,d] Guohua Xie,[a] Lisa S. Kölln,[a] Garry S. Hanan*,[c] Ifor D. W. Samuel*[a] and Eli Zysman-Colman*[b]

We show that the emission efficiency of blue-green phosphorescent emitters can be controlled through coupling of the excited state to vibrational modes. We controlled this vibrational coupling through choice of different ligands and as a result, complexes with CF_3-groups on the ancillary ligand were essentially non-emissive (Φ_{PL} < 1%), whereas with isosteric CH_3-groups the complexes were strongly emissive (Φ_{PL} > 50%). Emission of the complexes can be drastically improved (30 times higher Φ_{PL} compared to degassed solution for the CF_3-containing complexes) by blending them with an inert solid host such as PMMA, which mitigates metal-ligand vibrations. Solution-processed organic light-emitting diodes made from these materials showed efficiency as high as 6.3%.

[a] Organic Semiconductor Centre, SUPA, School of Physics and Astronomy, University of St. Andrews, St. Andrews, Fife, KY16 9SS, UK.
[b] Organic Semiconductor Centre, EaStCHEM School of Chemistry, University of St Andrews, St Andrews, Fife, KY16 9ST, UK.
[c] Département de Chimie, Université de Montréal, 2900 Edouard-Montpetit, Montréal, Québec H3T-1J4, Canada.
[d] Current address: Department of Chemistry, College of Sciences, University of Sharjah, P.O. Box 27272, Sharjah, United Arab Emirates.

Electronic Supplementary Information (ESI) available: [details of any supplementary information available should be included here]. See DOI: 10.1039/x0xx00000x

Journal Name

ARTICLE

Introduction

Iridium complexes have attracted significant attention as potent emitters in organic light-emitting diodes (OLEDs)[1-3] and light-emitting electrochemical cells (LEECs),[4-7] which are electroluminescent devices targeted for next generation flat panel displays and solid-state lighting. This is due to their high photoluminescence quantum yield (Φ_{PL}) and short radiative lifetime, facile colour tunability across the entirety of the visible spectrum, and good thermal and photo stability.[8] Importantly, both singlet and triplet excitons in these complexes contribute to device efficiencies,[9-12] which enables them to attain nearly 100% internal quantum efficiency.[13]

However, the reported OLEDs based on iridium complexes can in many cases show low device efficiency due to rapid non-radiative decay.[10,14,15] One reason for the reduced efficiencies observed is due to enhanced coupling of the excited state to vibrational modes.[10,14-16] Many different methods such as controlling isomer geometry or using rigid structures including inert hosts like poly(methylmethacrylate) (PMMA) and poly(styrene) have been reported for controlling the magnitude of vibrational coupling, which lead to moderate improvement of the quantum yield.[1,17] However, in order to establish a structure-property relationship for achieving both high Φ_{PL} and device efficiency, detailed photophysical and device studies on structurally related complexes are required. Here we show that blue-green cationic iridium(III) complexes of the form $[Ir(C^N)_2(N^N)]PF_6$ with the same cyclometallating, C^N, ligands but with different saturated strongly-donating guanidylpyridine (gpy) N^N ligands[18] can be used to control the emission efficiency. We find that there is severe quenching of PL in complexes with a CF_3 on the gpy ligand in solution, which we attribute to vibrational coupling. We show that this can be overcome by embedding the complex in an inert matrix. Therefore, we embedded the complexes within PMMA and observed a significant enhancement of the Φ_{PL} and emission lifetime, τ_e, compared to degassed MeCN solution. Quenching was further reduced at lower temperature. The devices fabricated using solution processing in a multilayer structure show efficiency of more than 6%.

Experimental

Materials and methods

Commercial chemicals were used as supplied. All reactions were performed using standard Schlenk techniques under inert (N_2) atmosphere with freshly obtained anhydrous solvents obtained from a Pure MBRAUN (MB-SPS) purification system except where specifically mentioned. Flash column chromatography was performed using silica gel (Silia-P from Silicycle, 60 Å, 40-63 µm). Analytical thin layer chromatography (TLC) was performed with silica plates with aluminum backings (250 µm with indicator F-254). Compounds were visualized under UV light. ^1H, ^{19}F and ^{13}C NMR spectra were recorded on a Brucker Avance 400 spectrometer at 400 MHz, 376 MHz and 100 MHz, respectively. The following abbreviations have been used for multiplicity assignments: “s” for singlet, “d” for doublet, “t” for triplet, “m” for multiplet and “br” for broad. Deuterated chloroform ($CDCl_3$), and deuterated acetonitrile (CD_3CN) were used as the solvent of record. Chemical shifts are reported in parts per million (ppm) relative to residual solvent ^1H resonance (1.96 ppm for CD_3CN, 7.26 ppm for $CDCl_3$) and the ^{13}C resonance (0.73 ppm and 118.69 ppm for CD_3CN, 77.00 ppm for $CDCl_3$) of the solvent. Melting points (Mp’s) were recorded using open-ended capillaries on a Meltemp melting point apparatus and are uncorrected. High-resolution mass spectra were recorded on a quadrupole time-of-flight (ESI-Q-TOF), model MICROTOF II from Bruker in positive electrospray ionization mode at the Université de Montreal. 1,3,4,6,7,8-Hexahydro-2H-pyrimido[1,2-*a*]pyrimidine (H-hpp), 2-bromo-5-(trifluoromethyl)pyridine, 2-bromo-5-methylpyridine, (±) BINAP, $Pd(OAc)_2$, *t*-BuOK were purchased from Aldrich and used as received. The corresponding iridium(III) dimers, $[Ir(C^N)_2Cl]_2$ were prepared according to the literature, where C^N is 2-phenylpyridinato (ppy) or 2-(4,6-difluorophenyl)-5-methylpyridinato (dFMeppy).[19]

Synthetic details

2,3,4,6,7,8-hexahydro-1-(5-methylpyridin-2-yl)-pyrimido[1,2-a]pyrimidine (Guanidyl-5-methyl-pyridine ***(Me-gpy) L1***): An oven-dried two-necked round bottomed flask was charged with (±)-BINAP (0.06 mmol, 0.038 g) and filled with nitrogen followed by multiple vacuum and then added 3 mL dry toluene to make a suspension of BINAP. The resulting suspension was heated at 90 °C for 5 min to dissolve the BINAP. This mixture was cooled to room temperature, $Pd(OAc)_2$ (0.04 mmol, 0.009 g) was added, and the mixture was stirred for 3 min. To the resulting bright yellow solution were added 2- bromo-5-methylpyridine (4 mmol, 0.688 g) and 1,3,4,6,7,8-hexahydro-2*H*-pyrimido[1,2-*a*]pyrimidine (4.3 mmol, 0.600 g) and stirred for 5 min at ambient temperature. The mixture turned into bright orange colour, to which was added *t*-BuOK (5.6 mmol, 0.640 g) and the flask was again charged with nitrogen followed by couple of vacuum. The reaction mixture was then stirred at 90 °C for 5 h, after which time it was cooled to room temperature and diethyl ether (60 mL) was added and the solution was filtered. Evaporation of the filtrate gave the ligand as a yellow oil liquid. Yield: 0.80 g (87%). The synthetic method was adopted from our previously reported protocol.[20] **^1H NMR (400 MHz, Chloroform-d) δ (ppm):** 8.07 (dd, *J* =1.6, 0.8 Hz, 1H), 7.51 (d, *J* = 8.5 Hz, 1H), 7.31 (dd, *J* = 2.4, 8.5 Hz, 1H), 3.82 (m, 2H), 3.39 (m, 2H), 3.22 (t, *J* = 6.1 Hz, 2H), 3.18 (t, *J* = 6.4 Hz, 2H), 2.21 (s, 3H), 2.03 (m, 2H), 1.86 (dd, *J* = 5.8, 11.7

Hz, 2H). **^{13}C NMR (101 MHz, Chloroform-d) δ (ppm):** 155.06, 150.39, 147.17, 137.26, 126.57, 119.30, 49.16, 48.91, 44.39, 44.21, 23.94, 23.08, 18.04. **HR-MS (ES-Q-TOF):** $[M]^+$ ($C_{13}H_{18}N_4$) calculated: 230.1531; experimental: 230.1528.

*1-(5-(trifluoromethyl)pyridin-2-yl)-2,3,4,6,7,8-hexahydro-pyrimido[1,2-a]pyrimidine (Guanidyl-5-trifluoromethyl-pyridine **(CF_3-gpy) L2**)*: Yield: 0.50 g (88%). The synthesis was carried out followed by the above method. **^{1}H NMR (400 MHz, Chloroform-d) δ (ppm):** 8.46 (d, *J* =0.8 Hz, 1H), 7.86 (d, *J* =9.0 Hz, 1H), 7.62 (dd, *J* = 2.5, 9.0 Hz, 1H), 3.96 (m, 2H), 3.45 (t, *J* = 5.7 Hz, 2H), 3.26 (t, *J* = 5.9 Hz, 2H), 3.20 (t, *J* = 6.3 Hz, 2H), 2.03 (m, 2H), 1.91 (m,2H). **^{19}F NMR (376 MHz, Chloroform-d) δ (ppm)**: -71.67. **^{13}C NMR (101 MHz, Chloroform-d) δ (ppm)**: 158.77, 149.43, 144.74, 144.69, 132.96, 117.00, 48.95, 48.80, 44.12, 43.41, 23.95, 22.80. **HR-MS (ES-Q-TOF):** $[M+H]^+$ ($C_{13}H_{16}F_3N_4$) calculated: 285.1329; experimental: 285.1323.

General procedure for the synthesis of $[Ir(C^N)_2(N^N)]PF_6$ complexes. Iridium dimer (0.07 mmol, 1.0 equiv.) and N^N ligand (Me-gpy or CF_3-gpy) (0.15 mmol, 2.10 equiv.) were solubilized with 20 mL of DCM/MeOH (50:50, v/v). The mixture was degassed by multiple vacuum and N_2 purging cycles. The suspension was heated at 50 °C for 19 h. The reaction mixture was cooled to room temperature and evaporated to dryness. The resulting solid was dissolved in a minimum amount of MeOH and a solution of NH_4PF_6 (10 equiv., 1.0 g / 10 mL) was added drop by drop to the methanolic solution to cause the precipitation of a solid. The suspension was cooled to 0 °C for 1 h, filtered and the resulting solid was washed with cold water. The crude solid was purified by flash chromatography on silica gel using DCM to DCM/Acetone (9/1, v/v).

$[Ir(ppy)_2(CF_3\text{-}gpy)]PF_6$, ***1a***. Light Yellow solid. Yield: 0.083 g (71 %). **Mp:** 179 °C. R_f : 0.25 (5% DCM/acetone on silica. **^{1}H NMR (400 MHz, Acetonitrile-d_3) δ (ppm):** 8.59 (d, *J* = 5.8 Hz, 1H), 8.27 (d, *J* = 6.0 Hz, 1H), 8.12 (t, *J* = 7.8 Hz, 3H), 7.97 (q, *J* = 7.8 Hz, 2H), 7.84 (s, 1H), 7.74 (dd, *J* = 16.0, 7.9 Hz, 2H), 7.56 (d, *J* = 9.0 Hz, 1H), 7.32 (t, *J* = 6.4 Hz, 1H), 7.26 (t, *J* = 6.7 Hz, 1H), 6.94 (dd, *J* = 15.6, 7.9 Hz, 2H), 6.80 (dt, *J* = 14.4, 7.4 Hz, 2H), 6.24 (d, *J* = 7.5 Hz, 1H), 6.16 (d, *J* = 7.6 Hz, 1H), 3.83 (m, 1H), 3.41 (m, 2H), 3.38 (m, 1H), 3.21 (m, 1H), 3.07 (dd, *J* = 10.9, 6.2 Hz, 2H), 2.85 (d, *J* = 13.3 Hz, 1H), 2.30 (m, 1H), 2.22 (s, 1H), 1.58 (d, *J* = 5.3 Hz, 1H), 1.15 (m, 1H). **^{19}F NMR (376 MHz, Acetonitrile-d_3) δ (ppm):** -63.45, -72.00, -73.87. **^{13}C NMR (101 MHz, Acetonitrile-d_3) δ (ppm):** 168.20, 157.86, 153.21, 152.34, 150.84, 149.68, 147.04, 145.05, 144.69, 138.90, 138.60, 136.92, 132.39, 132.15, 130.22, 129.97, 125.25, 124.58, 123.30, 122.99, 122.43, 122.12, 120.18, 119.88, 48.95, 48.60, 48.24, 46.86, 22.64. **HR-MS (ES-Q-TOF):** $[M\text{-}PF_6]^+$ ($C_{35}H_{31}F_3N_6Ir^+$) calculated: 785.2188; experimental: 785.2235.

$[Ir(ppy)_2(Me\text{-}gpy)]PF_6$, ***1b***. Light yellow solid. Yield: 0.089 g (74%). **Mp:** 164-165 °C. R_f : 0.20 (5% DCM/acetone on silica. **^{1}H NMR (400 MHz, Acetonitrile-d_3) δ (ppm):** 8.64 (d, *J* = 5.8 Hz, 1H), 8.36 (d, *J* = 5.4 Hz, 1H), 8.24 (d, *J* = 8.1 Hz, 1H), 8.19 (d, *J* = 8.1 Hz, 1H), 8.06 (t, *J* = 7.8 Hz, 2H), 7.90 (d, *J* = 7.8 Hz, 1H), 7.82 (dd, *J* = 13.1, 8.2 Hz, 2H), 7.50 (d, *J* = 8.5 Hz, 1H), 7.40 (d, *J* = 11.7 Hz, 2H), 7.33 (d, *J* = 7.0 Hz, 1H), 7.03 (dd, *J* = 17.5, 7.6 Hz, 2H), 6.89 (d, *J* = 6.3 Hz, 2H), 6.34 (d, *J* = 7.6 Hz, 1H), 6.25 (d, *J* = 7.5 Hz, 1H), 3.91 (d, *J* = 13.7 Hz, 1H), 3.53 (d, *J* = 18.9 Hz, 1H), 3.47 (m, 1H), 3.40 (m, 1H), 3.32 (m, 1H), 3.23 (m, 2H), 3.13 (d, *J* = 5.5 Hz, 1H), 3.03 (s, 1H), 2.38 (m, 1H), 2.05 (s, 3H), 1.61 (m, 1H), 1.13 (d, *J* = 5.3 Hz, 1H). **^{13}C NMR (101 MHz, Acetonitrile-d_3) δ (ppm):** 168.30, 153.91, 153.43, 153.14, 151.16, 150.84, 150.54, 149.07, 144.91, 141.26, 138.56, 138.29, 132.30, 131.72, 129.95, 125.32, 124.33, 123.10, 122.78, 121.92, 120.14, 119.65, 117.19, 48.79, 48.64, 48.33, 46.66, 22.96, 22.86, 16.80. **HR-MS (ES-Q-TOF):** $[M\text{-}PF_6]^+$ ($C_{35}H_{34}N_6Ir^+$) calculated: 731.2470; experimental: 731.2494.

$[Ir(dFMeppy)_2(CF_3\text{-}gpy)]PF_6$, ***2a***. Light red solid. Yield: 0.082 g (80%). **Mp:** 193 °C. R_f : 0.32 (5% DCM/acetone on silica. **^{1}H NMR (400 MHz, Acetonitrile-d_3) δ (ppm):** 8.38 (s, 1H), 8.27 (m, 2H), 8.18 (m, 2H), 7.88 (d, *J* = 8.2 Hz, 2H), 7.64 (m, 2H), 6.58 (dtd, *J* = 12.1, 9.6, 2.2 Hz, 2H), 5.76 (dd, *J* = 8.7, 2.3 Hz, 1H), 5.60 (dd, *J* = 8.9, 2.3 Hz, 1H), 3.85 (m, 1H), 3.42 (m, 2H), 3.28 (m, 1H), 3.21 (m, 1H), 3.16 (m, 1H), 3.09 (m, 1H), 2.86 (d, *J* = 13.2 Hz, 1H), 2.39 (s, 3H), 2.38 (s, 3H), 2.31 (m, 1H), 2.22 (m, 1H), 1.67 (s, 1H), 1.15 (t, *J* = 7.0 Hz, 1H). **^{19}F NMR (376 MHz, Acetonitrile-d_3) δ (ppm):** -64.60, -73.12 (m), -75.01, -110.57 (m), -110.93 (q, *J* = 9.3 Hz), -111.98 (t, *J* = 11.4 Hz), -112.93 (m). **^{13}C NMR (101 MHz, Acetonitrile-d_3) δ (ppm):** 157.69, 152.50, 151.27, 150.93, 146.94, 140.53, 140.38, 137.54, 134.40, 134.14, 123.56, 123.31, 123.09, 122.90, 118.51, 114.66, 114.43, 98.58, 98.37, 98.24, 98.03, 48.96, 48.62, 48.22, 47.22, 22.74, 22.62, 17.74, 17.34. **HR-MS (ES-Q-TOF):** $[M\text{-}PF_6]^+$ ($C_{37}H_{31}F_7N_6Ir^+$) calculated: 885.2124; experimental: 885.2258.

$[Ir(dFMeppy)_2(Me\text{-}gpy)]PF_6$, ***2b***. Lemon yellow solid. Yield: 0.097 g (81%). **Mp:** 180 °C. R_f : 0.22 (5% DCM/acetone on silica. **^{1}H NMR (400 MHz, Acetonitrile-d_3) δ (ppm):** 8.34 (s, 1H), 8.31 (d, *J* = 8.7 Hz, 1H), 8.23 (d, *J* = 9.5 Hz, 1H), 8.13 (s, 1H), 7.86 (s, 2H), 7.78 (d, *J* = 6.7 Hz, 1H), 7.43 (d, *J* = 8.5 Hz, 1H), 7.17 (s, 1H), 6.55 (dtd, *J* = 12.0, 9.5, 2.3 Hz, 2H), 5.74 (dd, *J* = 8.8, 2.3 Hz, 1H), 5.56 (dd, *J* = 8.9, 2.3 Hz, 1H), 3.82 (d, *J* = 13.5 Hz, 1H), 3.41 (m, 1H), 3.28 (d, *J* = 10.9 Hz, 1H), 3.23 (d, *J* = 9.0 Hz, 1H), 3.18 (dd, *J* = 7.5, 4.5 Hz, 2H), 3.14 (d, *J* = 9.6 Hz, 1H), 3.04 (m, 1H), 2.88 (d, *J* = 13.1 Hz, 1H), 2.37 (s, 3H), 2.36 (s, 3H), 2.28 (d, *J* = 4.5 Hz, 1H), 1.99 (s, 3H), 1.61 (m, 1H), 1.05 (m, 1H). **^{19}F NMR (376 MHz, Acetonitrile-d_3) δ (ppm):** -73.16, -75.04, -111.10 (q, *J* = 9.4 Hz), -111.38 (q, *J* = 9.4 Hz), -111.98 (m), -113.33 (m). **^{13}C NMR (101 MHz, Acetonitrile-d_3) δ** (ppm): 161.80, 157.86, 154.72, 153.65, 152.94, 151.31, 150.57, 149.10, 141.79, 140.16, 140.01, 134.01, 133.79, 132.29, 123.57, 123.38, 122.91, 122.71, 114.28, 114.11, 98.20, 97.95, 97.68, 48.80, 48.61, 48.32, 46.87, 30.36, 22.98, 17.88, 17.41, 16.83. **HR-MS (ES-Q-TOF):** $[M\text{-}PF_6]^+$ ($C_{37}H_{34}F_4N_6Ir^+$) calculated: 831.2407; experimental: 831.2514.

Table 1: *Photophysical properties of **1a-2b** in MeCN before and after degassing.*

	Before degassing					After degassing				
	Φ_{PL} (%)	λ_{max} (nm)	τ_e (μs)	k_r (s^{-1}) X 10^5	k_{nr} (s^{-1}) X10^6	Φ_{PL} (%)	λ_{max} (nm)	τ_e (μs)[a]	k_r(s^{-1}) X 10^5	k_{nr} (s^{-1}) X 10^6
1a	0.6 ± 0.1	512	0.026	2.3± 0.4	38.2± 6.4	2.8 ± 0.3	512	0.09, 1.60	-	-
1b	0.9 ± 0.1	512	0.031	2.9± 0.3	32.0± 3.6	50.8 ± 4.0	510	1.90	2.7 ± 0.2	0.26 ± 0.02
2a	1.0 ± 0.1	468, 495	0.040	2.5± 0.3	24.8± 2.5	1.7 ± 0.2	462, 510	0.11, 0.98	-	-
2b	1.2 ± 0.1	470, 497	0.047	2.6± 0.2	21.0± 1.8	65.6 ± 5.0	470, 496	2.60	2.5 ± 0.2	0.13 ± 0.01

[a] See ESI for details of bi-exponential decay processes in **1a** and **2a**.

Results and discussion

Photophysical characterisation

The complexes under study are based on gpy N^N ligands,[21] which are strongly donating compared to traditional diimine ligands such as 2,2'-bipyridine and coordinate to a wide variety of metal ions,[20,22-25] including iridium (**Fig. 1**).[18] Complexes **1a,b–2a,b** were prepared in 71–-81% yield. The desired complexes were synthesised by allowing one equivalent of Ir dimer, $[Ir(C^N)_2Cl]_2$ to react with a gpy ligand containing a CF_3 group, gpy-CF_3, (**1a** and **2a**) or a CH_3 group, gpy-Me, (**1b** and **2b**).

The photophysical properties of these four complexes were measured in both aerated and degassed MeCN. The photoluminescence (PL) spectra in aerated solution are shown in **Fig. 2(a)** while the PL decay traces are shown in **Fig. 2(b)**; Φ_{PL} values, PL lifetime (τ_e) and calculated radiative (k_r) and non-radiative decay (k_{nr}) rate constants are given in **Table 1**. The analysis shows that all four complexes have similar respective Φ_{PL}, k_r and k_{nr} prior to degassing.

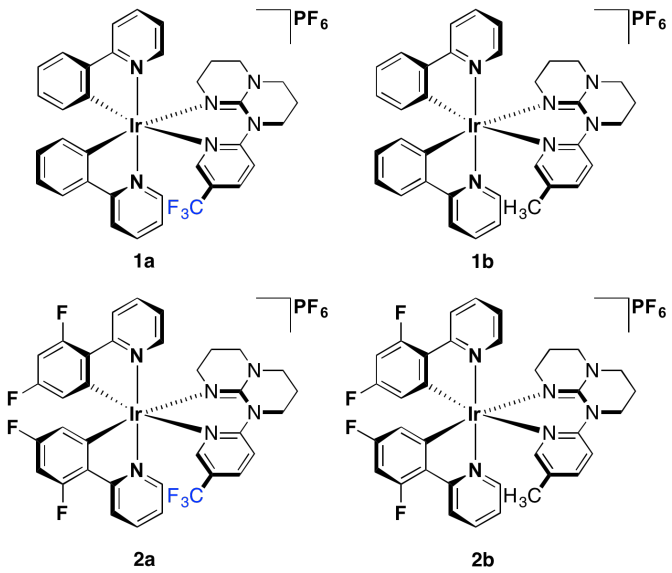

Figure 1: Complexes under investigation in this study.

Upon degassing the solutions, a dramatic divergence in photophysical behaviour is observed between **1a**/**2a** and **1b**/**2b**. The Φ_{PL} values are more than 50% for **1b** and **2b**, but remain around 2% for **1a** and **2a**. The PL decays for **1b** and **2b** are monoexponential, with τ_e ~ 2 μs (**Fig. 3** and **Table S1**), typical for cationic iridium complexes.[26-28] By contrast, the PL decays of **1a** and **2a** are biexponential, with the average τ_e < 300 ns (**Fig. 3** and **Table S1**). Upon degassing, k_r shows essentially no net change for **1b/2b**, while k_{nr} decreases by two orders of magnitude. We attribute the low Φ_{PL} values observed for **1a** and **2a** to strong vibrational coupling[10,14,16] principally among the asymmetric stretching modes of the Ir-N_{dFppy} bonds and the asymmetric stretching modes of the C-N and C-C bonds of the pyridine ring of the CF_3-gpy in **1a**and **2a**.

This hypothesis is corroborated by DFT calculations where the LUMO (lowest unoccupied molecular orbital) is switched from the CF_3-gpy moiety in **2a** to the pyridine unit of the C^N ligands in **2b** (**Fig. 4**); a similar relationship exists for **1a/1b** (**Fig. S20**). With the presence of more electron-withdrawing fluoro substituents, the emission profiles of complexes **2a** and **2b** are expectedly blue-shifted compared to those of **1a** and **1b**. The emission spectra of **1a** and **1b** are broad and featureless, indicative of a mixed ^{3}CT emission while the spectra of **2a** and **2b** are structured, suggesting a significant ^{3}LC-based emission. Unrestricted DFT calculations support this assignment as they show the triplet state spin density is principally localised on both the Ir(III) centre and the C^N ligands for all complexes, but to some extent is also delocalised onto the guanidyl part of the ancillary CH_3-/CF_3-gpy ligand in complexes **1a** and **1b**, which is not the case for complexes **2a** and **2b** (Fig. **5**).

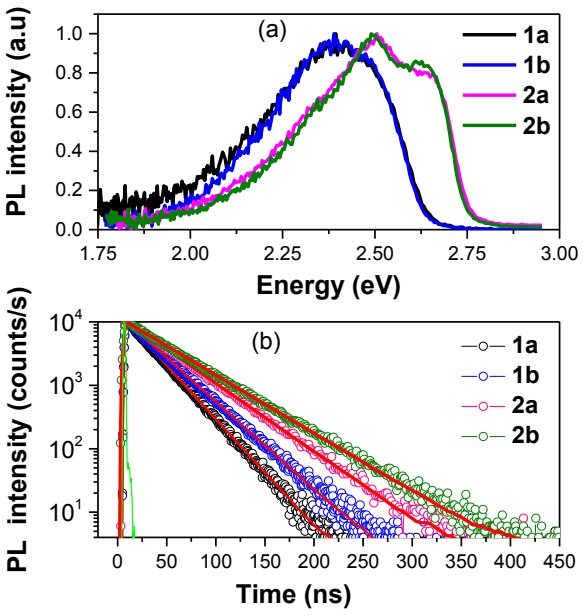

Figure 2: Emission spectra of **1a–2b** in MeCN in air (λ_{exc} = 360 nm). (b) Photoluminescence decay of **1a–2b** in MeCN in air (λ_{exc} = 375 nm). The experimental data was fitted to a monoexponential decay (red lines).

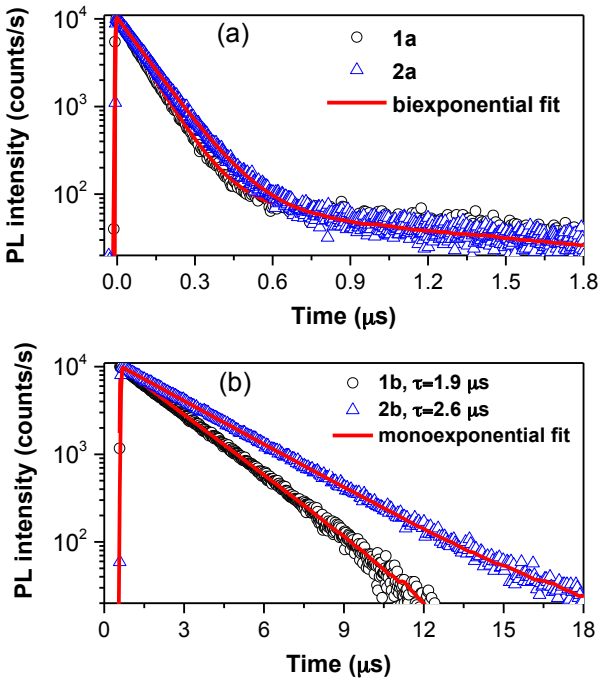

Figure 3: Photoluminescence decay of (a) **1a** and **2a** and (b) **1b** and **2b** in degassed MeCN solution. λ_{exc} = 375 nm. fits are shown in red.

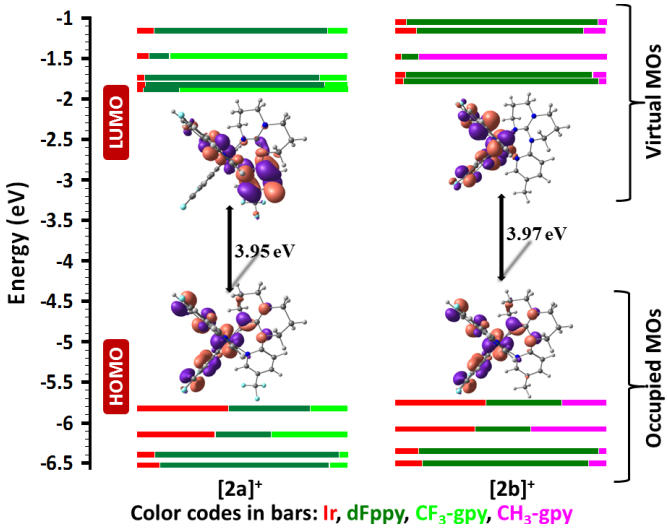

Figure 4*:* Calculated frontier MO energies of $[\mathbf{2a}]^+$ and $[\mathbf{2b}]^+$, obtained from DFT [(B3LYP/SBKJC-VDZ for Ir(III)) and (6-31g** for C,H,N,F] with CPCM(CH_3CN) and 0.5 eV threshold of degeneracy (isovalued at 0.03). Kohn-Sham MOs of $[\mathbf{2a}]^+$ and $[\mathbf{2b}]^+$ are also shown.

Frequency calculations suggest that there is a strong coupling among the asymmetric stretching modes of the Ir-N_{dFppy} bonds and the asymmetric stretching modes of the C-N and C-C bonds of the pyridine ring of the CF_3-gpy ligand in **2a** (vibrational mode #121, E = 1054 cm^{-1}) (see **Table S4** for other minor contributing vibrational modes that couple with the spin density). This coupling is found to be very weakly present in **2b**, the analog complex containing CH_3-gpy. Thus, the strong vibrational coupling present in the T_1 state leads to poor Φ_{PL} for **2a** (**1a**) and not for **2b** (**1b**).

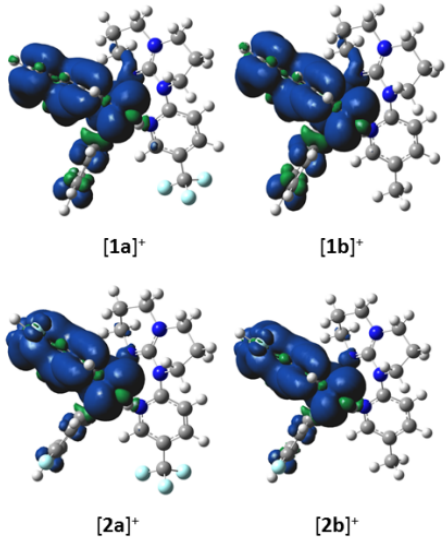

Figure 5. Triplet spin density distributions of complexes $[\mathbf{1a}]^+$, $[\mathbf{1b}]^+$, $[\mathbf{2a}]^+$ and $[\mathbf{2b}]^+$, obtained from TD-DFT [(UB3LYP/SBKJC-VDZ for Ir(III)) and (6-31g** for C,H,N,F] with CPCM(MeCN) (isovalue at 0.02).

This vibrational coupling can be quantified by analysis of the Huang-Rhys factors which were estimated from the relative strength of (0,1) and (0,0) transitions. Complexes **2a** and **2b** have well-defined 0–0 and 0–1 peaks in their degassed PL spectra while this is not the case for **1a** and **1b**. Therefore, we used **2a** and **2b** to further investigate the nature of this vibrational coupling. From the analysis there is stronger vibrational coupling in **2a** (Huang Rhys factor = 1.14) compared to **2b** (Huang Rhys factor = 1.09).

For electroluminescence applications, an emitter with a high Φ_{PL} in the solid state is required. Previously it has been shown that the Φ_{PL} can be improved by blending the emissive complex within an inert solid host.[14,29] Therefore, we blended our complexes with PMMA to modulate the vibrational coupling in order to enhance the emission efficiency of the complexes. The photophysical data is shown in **Table S3** (ESI). Both **2a** and **2b** show relatively high Φ_{PL} in thin film, with a notable recovery of Φ_{PL} for **2a** measured in air (> 65%) and under an N_2 environment (> 72%) given that **2a** was only slightly emissive (1.7%) in degassed solution.

We undertook temperature-dependent photophysical studies in order to comprehend further the contrasting behaviour of **2a** in solution and thin film. A comparison of the PL emission of 2 wt% **2a** in PMMA at room temperature and at 77 K (λ_{exc} = 380 nm) is shown in **Fig. 6(a)**. It can be seen that the 0-0 and 0-1 peaks are more prominent in the solid-state spectrum at room temperature compared to the degassed MeCN solution spectrum (**Fig. S18(b)**). This shows that having the complex embedded in the host PMMA inhibits significantly the vibrational coupling of the CF_3-moiety associated with the non-radiative decay of the PL emission. At 77 K the 0–0 peak becomes even more prominent (Huang Rhys factor = 1.05) due to reduced vibrational coupling compared to the measurements at 300 K (Huang Rhys factor = 1.15) and in MeCN

degassed solution spectra (Huang Rhys factor = 1.14). Moreover, relative intensity of PL emission increases at 77 K.

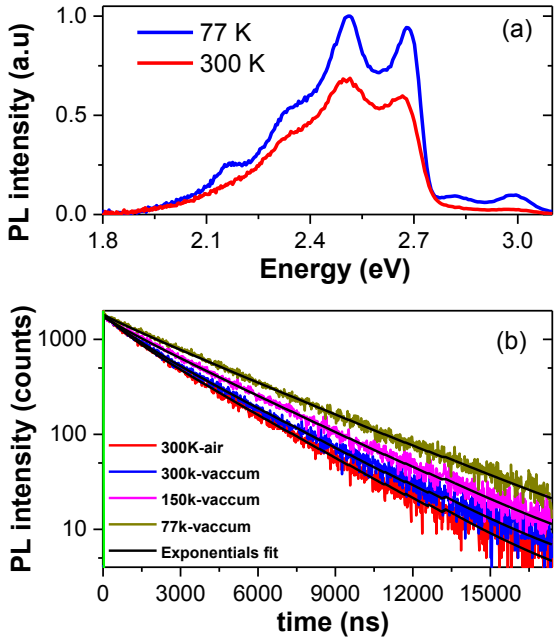

Figure 6: (a) PL spectra of 2 wt% **2a** in PMMA measured at 300 K and 77 K (λ_{exc} = 380 nm). (b) Temperature-dependent PL decay of 2 wt% **2a** in PMMA measured in air and under vacuum (λ_{exc} = 379 nm) with fits shown in black.

The transient PL decays of 2 wt% **2a** in PMMA at different temperatures and in different environments (air and vacuum) are shown in **Fig. 6(b)** and the photophysical data collected in **Table 2** and **Table S2**. Both components of the decay of **2a** under vacuum are longer-lived than under air due to the absence of O_2, which quenches phosphorescence. The τ_e increases upon cooling, to 3.2 µs at 150 K and 3.7 µs at 77 K due to suppression of thermally-activated non-radiative processes,[15] including the coupling of the excited state to vibrational modes. Furthermore, the lifetime measured in the solid state is more than 15 times longer than that in degassed MeCN. This shows that doping **2a** into PMMA significantly reduces the vibrational quenching at room temperature and this vibrational quenching is almost completely absent at 77 K.

Table 2: *Photophysical properties of **2a** in DCM and 2 wt% of **2a** in PMMA thin film* measured at room temperature (300 K)

2a	**DCM**		**Film**	
	Before degassing	After degassing	Air	Vacuum
Φ_{PL} (%)	1.0	1.7	65.9	72.4
τ_e (µs)[a]	0.04	0.11, 0.98	0.82, 2.80	0.92, 3.00

[a] See ESI for details of bi-exponential decay processes.

Device fabrication

After controlling the vibrational coupling in the solid state, we investigated the electroluminescence of **2a** and **2b** by fabricating solution-processed organic light emitting diodes (OLEDs). For comparison, we also fabricated OLEDs with **1b**. The device architecture consisted of following layers: ITO / PEDOT:PSS (30 nm) / PVK (30 nm) / mCP:OXD7:**1b–2b**(75:20:5 wt%) (30 nm) / B3PYMPM (60 nm) / Ca (20 nm) / Al (100 nm). Here poly(3,4-ethylenedioxythiophene):poly(styrene sulfonate) (PEDOT:PSS) is the hole injection layer and was spin-coated at 4000 rpm for 60 s and then baked it at 120 ^{0}C for 20 minutes to obtain a 35 nm smooth film. Poly(*N*-vinylcarbazole) (PVK) was used as the hole transporting layer. PVK was spin-coated from chlorobenzene at 2000 rpm inside the nitrogen-filled glovebox. It was then baked at 80 ^{0}C for 2h to form a smooth film of 30 nm thickness. The emitting layer consisted of 1,3-bis(*N*-carbazolyl)benzene (mCP) and 2,2′-(1,2-phenylene)bis[5-(4-*tert*-butylphenyl)-1,3,4-oxadiazole] (OXD-7) as host materials and phosphorescent dopants **1b–2b**, which were cast from acetonitrile at 2000 rpm to form a film of 30 nm thickness. OXD7 and mCP are wide band gap (3.7 eV) materials.[30, 31] OXD7 and mCP were selected because they are wide band gap materials with high triplet energies and together can transport both electron and hole well. A 60 nm electron-transporting layer 4,6-bis(3,5-di(pyridin-3-yl)phenyl)-2-methylpyrimidine (B3PyMPM) was then thermally evaporated onto the emitting layer under high vacuum. Finally, the composite cathode Ca (20 nm) / Al (100 nm) was thermally deposited through a shadow mask in the vacuum chamber at ~ 2.0×10^{-6} mbar. The device architecture along with the energy levels are shown in **Fig. 7**. The electroluminescence (EL) spectra of the three devices are shown in **Fig. 8(a)**. EL spectra of **2a** and **2b** are similar to their PL spectra but are red-shifted and show different relative intensities of the vibronic peaks. However, the EL spectrum of **1b** has two distinct vibronic peaks compared to PL spectra, which showed only one broad peak, pointing to a greater ligand-centered character to the emission of **1b** in the device. In the EL spectra, we did not observe any emission around 410 nm (expected emission from host) due to complete energy transfer from the host to the iridium emitters.[32] Current-voltage characteristics of the devices are shown in **Fig. 8(b)**.

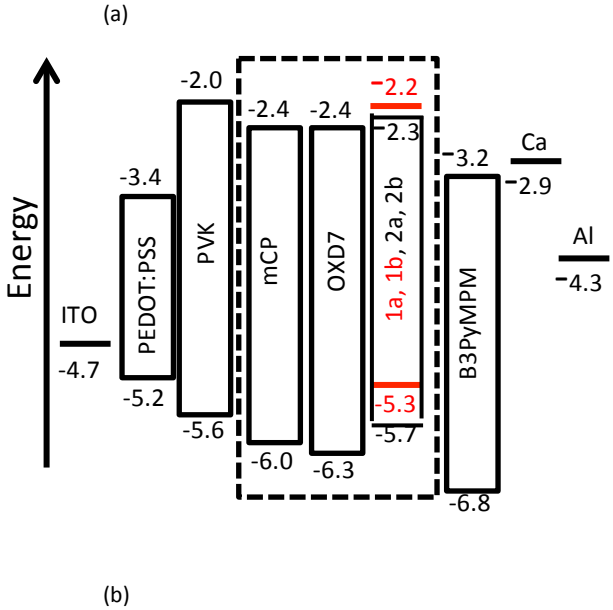

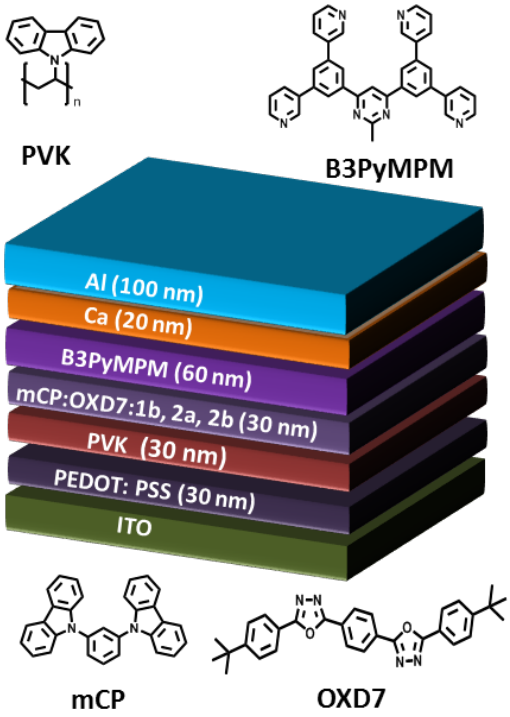

Figure 7: (a) Energy level diagram of light emitting devices using **1b–2b** as the emitter. (b) Schematic of fabricated light emitting devices fabricated using **1b-2b**.

The device made from **1b** showed the highest current density at high voltage (> 6 V), followed by the devices with **2b** then **2a**. The turn-on voltage for the OLED with **2a** is lower than that with **2b**.

All devices show a steep increase in luminance with voltage once turned on (see **Fig. 8(c)**). A maximum luminance of 1846 cd/m^2 at a driving voltage of 10 V, 881 cd/m^2 at 15.1 V and 332 cd/m^2 at 15.1 V was achieved for **1b**, **2a** and **2b**, respectively. The luminance characteristics of the devices (Fig. **8 (c)**) show that the OLED based on **1b** has the lowest turn-on voltage and highest power and current efficiencies among all devices whereas **2b** has the highest turn-on voltage. The external quantum efficiencies (EQE) of the devices are given in **Fig. 8(d)**. The EL properties are summarized in **Table 3**.

The maximum EQE of 6.5% was obtained for **1b** at a luminance of 41 cd/m^2 (7V), which reduced only slightly to 6.3% at 100 Cd/m^2 and 5.8% at 1000 Cd/m^2. A similar low roll off of the EQE for **2a** and **2b** was also observed. A maximum EQE of 2.4% at luminance of 35 cd/m^2 was obtained for **2a**, which reduced to 2.3% at 100 Cd/m^2, whereas in the case of **2b**, a maximum EQE of 3.0% was obtained at 40 cd/m^2, which reduced to 2.8% at 100 Cd/m^2.

The EQE of 6.3% and current efficiency of 20.8 Cd/m^2 at a luminance of 100 cd/m^2 for **1b** is among the best performing OLEDs based on the use of cationic iridium complexes as emissive layer.[33-39] To the best of our knowledge the best performing solution-processed device using a cationic iridium complex as the emitter showed a maximum EQE of 7.1% and CE of 10.0 cd/m^2.[39] This device used [Ir(npy)$_2$(c-phen)]PF$_6$, (npy is 2-(naphthalen-1-yl)pyridinato c-phen = 1-Ethyl-2-(9-(2-ethylhexyl)-9*H*-carbazol-3-yl)-1*H*-imidazo[4,5-f][1,10]phenanthroline). Due to the use of strongly conjugated C^N ligands the emission colour of the device was in the red region with CIE coordinates of (0.57, 0.40)[39] and so a direct comparison to the current devices is not appropriate. Recently, Duan and co-workers reported the use of the blue-green [Ir(ppy)$_2$(pzpy)][PF$_6$] (pzpy = 2-(1Hpyrazol-1-yl)pyridine) complex as the emitter in a a single-layer solution-processed OLED.[40] A maximum EQE of 6.8% with current efficiency of 17.1 cd/m^2 was obtained with CIE coordinates of (0.21, 0.48).

Table 3: *Electroluminescence characteristics of the OLEDs.*

Emitter	V_{on} [a] (V)	λ_{peak} [b] (nm)	EQE[c] (%)	CE[d] (cd/A)	PE[e] (lm/W)	CIE[f]
1b	5.8	527	6.3	20.8	8.7	(0.29, 0.58)
2a	6.3	506	2.3	6.2	1.9	(0.26, 0.47)
2b	7.8	503	2.8	7.1	1.6	(0.22,0.43)

[a] Turn-on voltage @ 1 cd/m^2. [b] Peak wavelength at 1 mA/cm^2. [c] External quantum efficiency at 100 cd/m^2. [d] Current efficiency at 100 cd/m^2. [e] Power efficiency at 100 cd/m^2. [f] The Commission Internationale de L'Eclairage (CIE) coordinates at 1 mA/cm^2.

Our device using **1b** has CIE coordinates of (0.29, 0.58) and so is slightly red-shifted and has a slightly higher current efficiency compared to the device of Duan *et al.* The device with **1b** exhibits considerably better performance. We attribute this to the shallower HOMO enabling more efficient hole injection, which explains the lower turn-on voltage and improved charge balance and device efficiency. The device with **2a** has the lowest EQE, despite a higher luminance and similar power efficiency compared to **2b** (**Fig. 8(d)** and **8 (e)**). These results suggest there may be poorer charge carrier balance in these devices.[17, 32, 41]

Conclusions

In summary, we have shown that the suppressed emission of CF$_3$-containing complexes **1a** and **2a** in MeCN solution can be overcome by decreasing the temperature or by embedding these complexes in a rigid PMMA matrix. In fact, emission in the thin film is enhanced by ca. 30-fold compared to measurement in degassed solution. The supressed emission in solution is the result of strong coupling of the excited state to vibrational modes implicating the CF$_3$-group; whereas **1a** and **2a** show Φ_{PL} of <1%, replacement of the CF$_3$- group by CH$_3$- recovers the emission without affecting the emission energy, with Φ_{PL} >50%. OLEDs were made with both solution-state emissive (**2b**) and non-emissive complexes (**2a**). Their performance resulted in similar EQEs measured for both devices. Thus, this study demonstrates the importance of assessing the solid-state optoelectronic properties of emitters prior to their considered use in EL devices.

Journal Name

ARTICLE

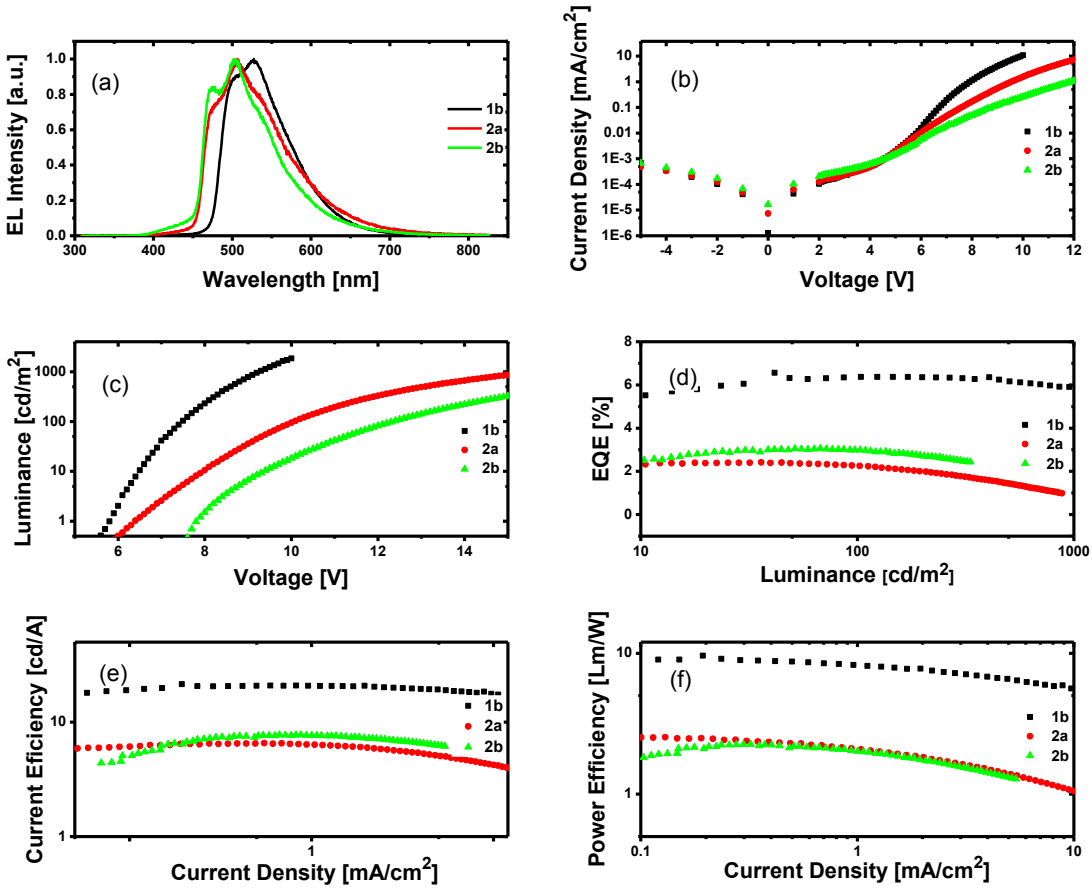

Figure 8. (a) EL spectra of three complexes. (b) Current density of **1b** (black), **2a** (red) and **2b** (green) as function of voltage of OLEDs. (c) Luminance as a function of applied voltage. (d) External quantum efficiency (EQE) as a function of Luminance. (e) Current efficiency as a function of current density. (f) Power efficiency as a function of current density for the devices fabricated using **1b**, **2a** and **2b**.

Acknowledgements

We are grateful to the European Research Council (grant 321305), EPSRC (grants EP/J01771X, EP/L017008/1 and EP/M02105X/1) for financial support. IDWS acknowledges a Royal Society Wolfson Research Merit Award. GSH thanks the Natural Sciences and Engineering Research Council (NSERC) of Canada for funding.

Notes and references

1. Y. You and S. Y. Park, *Dalton Trans.*, 2009, 1267-1282.
2. L. Xiao, Z. Chen, B. Qu, J. Luo, S. Kong, Q. Gong and J. Kido, *Adv. Mater.*, 2011, **23**, 926-952.
3. H. Xu, R. Chen, Q. Sun, W. Lai, Q. Su, W. Huang and X. Liu, *Chem. Soc. Rev.*, 2014, **43**, 3259-3302.
4. R. D. Costa, E. Ortí, H. J. Bolink, F. Monti, G. Accorsi and N. Armaroli, *Angew. Chem. Int. Ed.*, 2012, **51**, 8178-8211.
5. T. Hu, L. He, L. Duan and Y. Qiu, *J. Mater. Chem.*, 2012, **22**, 4206-4215.
6. M. S. Lowry and S. Bernhard, *Chem. Eur. J.*, 2006, **12**, 7970-7977.
7. A. F. Henwood and E. Zysman-Colman, *Top. Curr. Chem.*, 2016, **374**, 1-41.
8. S. Ladouceur and E. Zysman-Colman, *Eur. J. Inorg. Chem.*, 2013, **2013**, 2985-3007.
9. M. A. Baldo, D. O'brien, Y. You, A. Shoustikov, S. Sibley, M. Thompson and S. Forrest, *Nature*, 1998, **395**, 151-154.
10. S.-C. Lo, R. E. Harding, C. P. Shipley, S. G. Stevenson, P. L. Burn and I. D. Samuel, *J. Am. Chem. Soc.*, 2009, **131**, 16681-16688.
11. M. Baldo, M. Thompson and S. Forrest, *Nature*, 2000, **403**, 750-753.

12. X. Gong, W. Ma, J. C. Ostrowski, G. C. Bazan, D. Moses and A. J. Heeger, *Adv. Mater.*, 2004, **16**, 615-619.
13. C. Adachi, M. A. Baldo, M. E. Thompson and S. R. Forrest, *J. Appl. Phys.*, 2001, **90**, 5048-5051.
14. R. E. Harding, S.-C. Lo, P. L. Burn and I. D. Samuel, *Org. Electron.*, 2008, **9**, 377-384.
15. T. Sajoto, P. I. Djurovich, A. B. Tamayo, J. Oxgaard, W. A. Goddard III and M. E. Thompson, *J. Am. Chem. Soc.*, 2009, **131**, 9813-9822.
16. J. A. Treadway, B. Loeb, R. Lopez, P. A. Anderson, F. R. Keene and T. J. Meyer, *Inorg. Chem.*, 1996, **35**, 2242-2246.
17. J. Lee, H.-F. Chen, T. Batagoda, C. Coburn, P. I. Djurovich, M. E. Thompson and S. R. Forrest, *Nat. Mater.*, 2016, **15**, 92-98.
18. K. Hasan, A. K. Pal, T. Auvray, E. Zysman-Colman and G. S. Hanan, *Chem. Commun.*, 2015, **51**, 14060-14063.
19. M. Nonoyama, *Bull. Chem. Soc. Jpn.*, 1974, **47**, 767-768.
20. A. K. Pal, S. Nag, J. G. Ferreira, V. Brochery, G. La Ganga, A. Santoro, S. Serroni, S. Campagna and G. S. Hanan, *Inorg. Chem.*, 2014, **53**, 1679-1689.
21. A. K. Pal, P. K. Mandali, D. K. Chand and G. S. Hanan, *Synlett*, 2015, **26**, 1408-1412.
22. S. Nag, J. G. Ferreira, L. Chenneberg, P. D. Ducharme, G. S. Hanan, G. La Ganga, S. Serroni and S. Campagna, *Inorg. Chem.*, 2010, **50**, 7-9.
23. A. K. Pal, P. D. Ducharme and G. S. Hanan, *Chem. Commun.*, 2014, **50**, 3303-3305.
24. A. K. Pal, S. Serroni, N. Zaccheroni, S. Campagna and G. S. Hanan, *Chem. Sci.*, 2014, **5**, 4800-4811.
25. A. K. Pal, N. Zaccheroni, S. Campagna and G. S. Hanan, *Chem. Commun.*, 2014, **50**, 6846-6849.
26. S. Ladouceur, D. Fortin and E. Zysman-Colman, *Inorg. Chem.*, 2011, **50**, 11514-11526.
27. L. He, L. Duan, J. Qiao, R. Wang, P. Wei, L. Wang and Y. Qiu, *Adv. Funct. Mater.*, 2008, **18**, 2123-2131.
28. R. D. Costa, E. Ortí, H. J. Bolink, S. Graber, S. Schaffner, M. Neuburger, C. E. Housecroft and E. C. Constable, *Adv. Funct. Mater.*, 2009, **19**, 3456-3463.
29. T. Sajoto, P. I. Djurovich, A. Tamayo, M. Yousufuddin, R. Bau, M. E. Thompson, R. J. Holmes and S. R. Forrest, *Inorg. Chem.*, 2005, **44**, 7992-8003.
30. D. O'Brien, A. Bleyer, D. Lidzey, D. Bradley and T. Tsutsui, *J. appl. Phys.*, 1997, **82**, 2662-2670.
31. K. Masui, H. Nakanotani and C. Adachi, *Org. Electron.*, 2013, **14**, 2721-2726.
32. A. F. Henwood, A. K. Bansal, D. B. Cordes, A. M. Slawin, I. D. Samuel and E. Zysman-Colman, *J. Mater. Chem. C*, 2016, **4**, 3726-3737
33. E. A. Plummer, A. van Dijken, J. Hofstraat, L. De Cola and K. Brunner, *Adv. Funct. Mater.*, 2005, **15**, 281-289.
34. W. Y. Wong, G. J. Zhou, X. M. Yu, H. S. Kwok and Z. Lin, *Adv. Funct. Mater.*, 2007, **17**, 315-323.
35. L. He, L. Duan, J. Qiao, D. Zhang, G. Dong, L. Wang and Y. Qiu, *Org. Electron.*, 2009, **10**, 152-157.
36. L. He, L. Duan, J. Qiao, D. Zhang, L. Wang and Y. Qiu, *Org.Electron.*, 2010, **11**, 1185-1191.
37. B. Park, Y. H. Huh, H. G. Jeon, C. H. Park, T. K. Kang, B. H. Kim and J. Park, *J. Appl. Phys.*, 2010, **108**, 094506.
38. G. Nasr, A. Guerlin, F. Dumur, L. Beouch, E. Dumas, G. Clavier, F. Miomandre, F. Goubard, D. Gigmes and D. Bertin, *Chem. Commun.*, 2011, **47**, 10698-10700.
39. H. Tang, Y. Li, B. Zhao, W. Yang, H. Wu and Y. Cao, *Org. Electron.*, 2012, **13**, 3211-3219.
40. D. Ma, C. Zhang, Y. Qiu and L. Duan, *J. Mater. Chem. C*, 2016, **4**, 5731-5738
41. M. Y. Wong, G. Xie, C. Tourbillon, M. Sandroni, D. B. Cordes, A. M. Slawin, I. D. Samuel and E. Zysman-Colman, *Dalton Trans.*, 2015, **44**, 8419-8432.

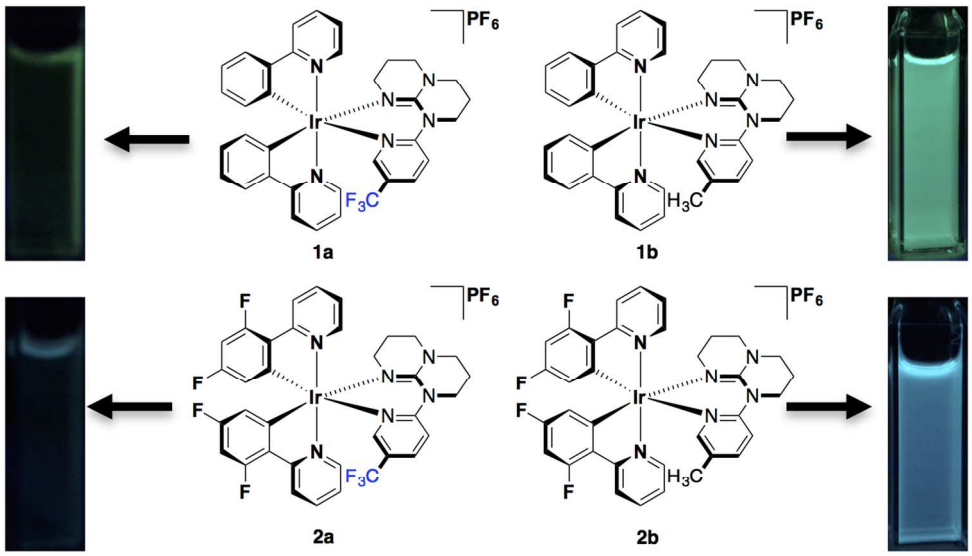
PF6
Ir
N
F3C
H3C
F
1a
1b
2a
2b

Controlling the emission of blue-green Iridium (III) phosphorescent emitters

Muhammad T. Sajjad,[a] Nidhi Sharma,[a,b] Amlan K. Pal,[b] Kamrul Hasan,[c,d] Guohua Xie,[a] Lisa Sophie Kölln,[a] Garry S. Hanan,*[c] Ifor D. W. Samuel,*[a] Eli Zysman-Colman*[b]

[a] Organic Semiconductor Centre, SUPA, School of Physics and Astronomy, University of St. Andrews, St. Andrews, Fife, KY16 9SS, UK*; Tel: +44-1334 463114;*
E-mail: idws@st-andrews.ac.uk

[b] Organic Semiconductor Centre, EaStCHEM School of Chemistry, University of St Andrews, St Andrews, Fife, UK, KY16 9ST, *Fax: +44-1334 463808; Tel: +44-1334 463826;*
E-mail: eli.zysman-colman@st-andrews.ac.uk; URL: http://www.zysman-colman.com

[c] Département de Chimie, Université de Montréal, 2900 Edouard-Montpetit, Montréal, Québec H3T-1J4, Canada.
E-mail: garry.hanan@umontreal.ca; Fax: +1-514 343-2468; Tel: +1-514 343-7056

[d] Department of Chemistry, College of Sciences, University of Sharjah, P. O. Box 27272, Sharjah, United Arab Emirates
E-mail: *khasan@sharjah.ac.ae*; *Fax:* +971 6 5053820; *Tel:* +971 6 5166768

SUPPORTING INFORMATION

Table of contents

^{1}H, ^{19}F and ^{13}C NMR spectra of individual compounds and complexes

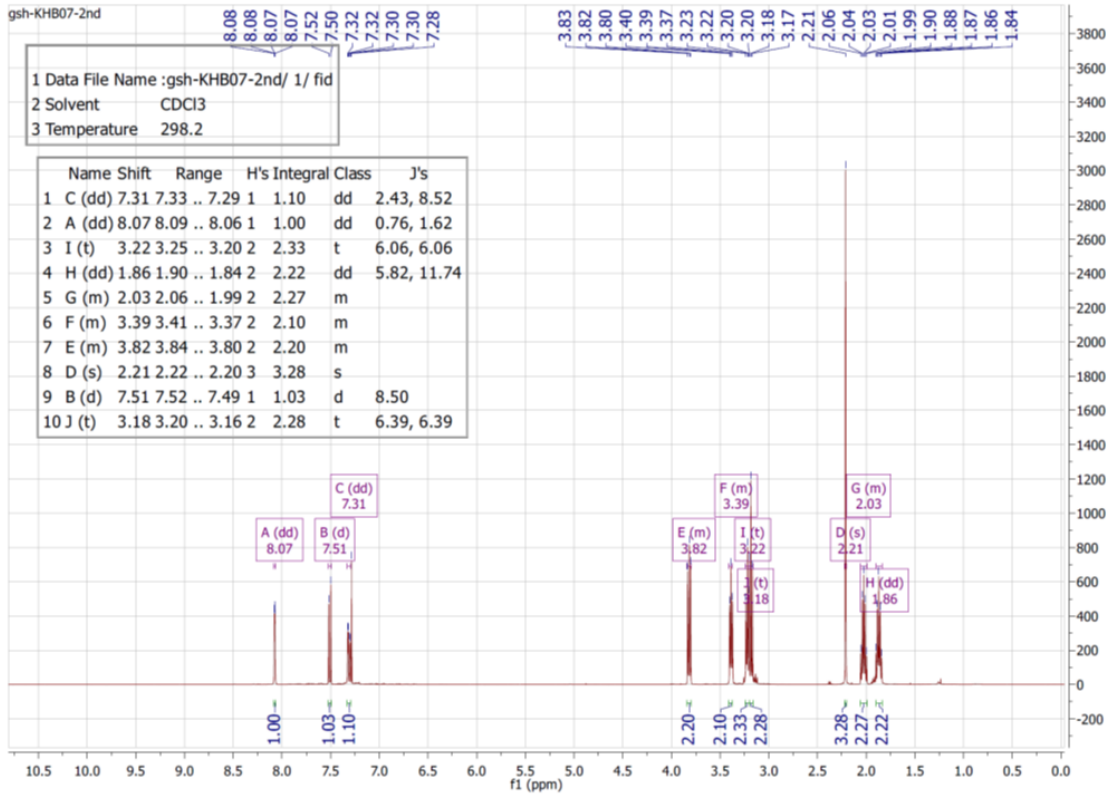

Figure **S1**. ^{1}H NMR spectrum of **L1 (Me-gpy)** in $CDCl_3$ at 400 MHz.

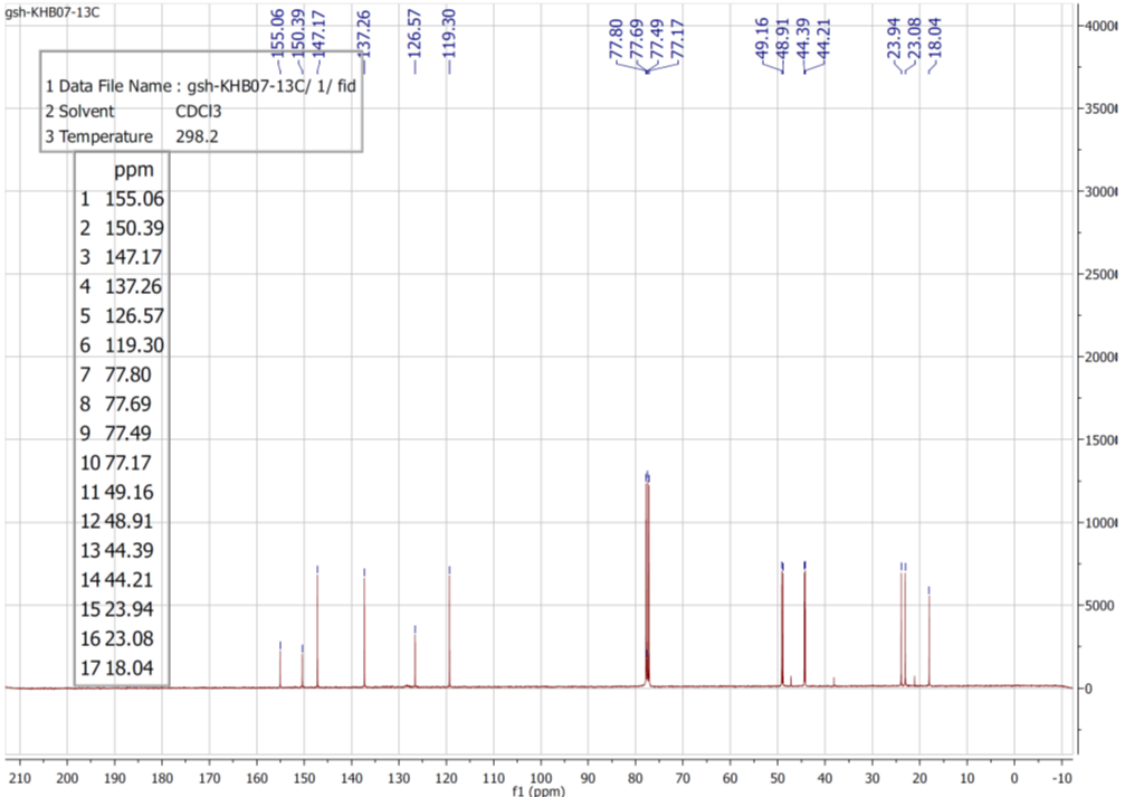

Figure **S2**. ^{13}C NMR spectrum of **L1 (Me-gpy)** in $CDCl_3$ at 400 MHz.

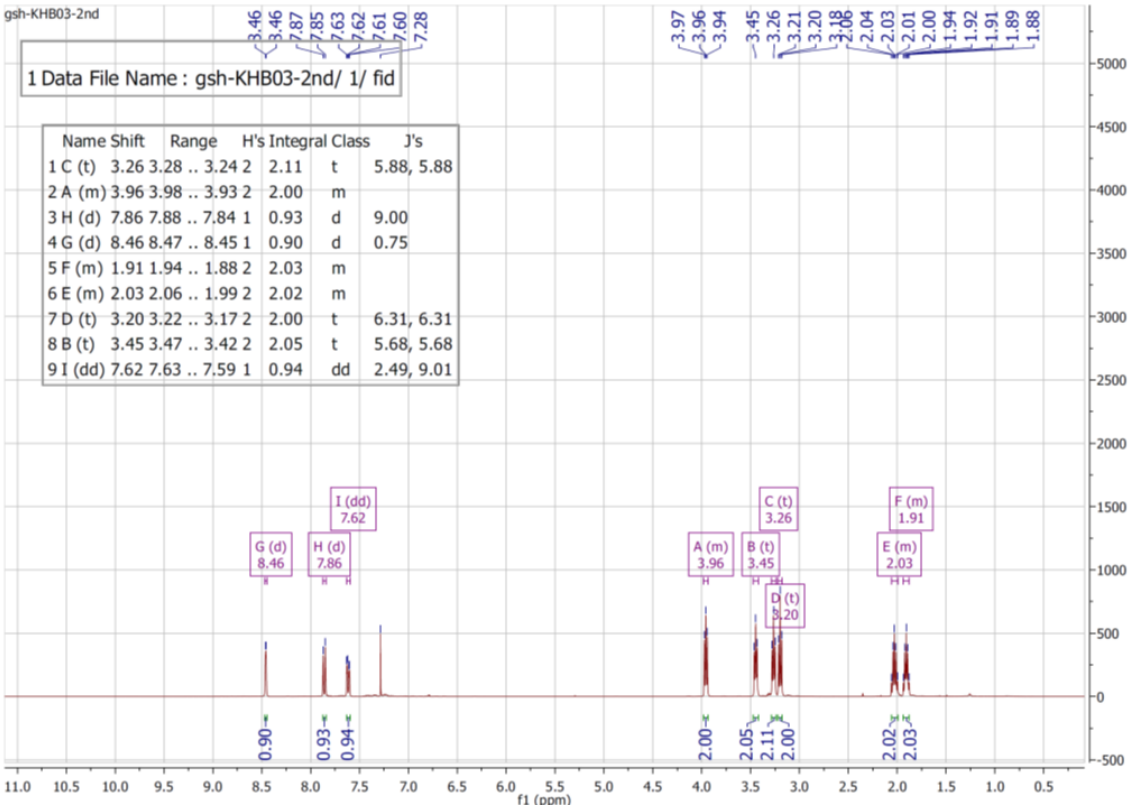

Figure **S3**. ^{1}H NMR spectrum of **L2 (CF_3-gpy)** in $CDCl_3$ at 400 MHz at r.t.

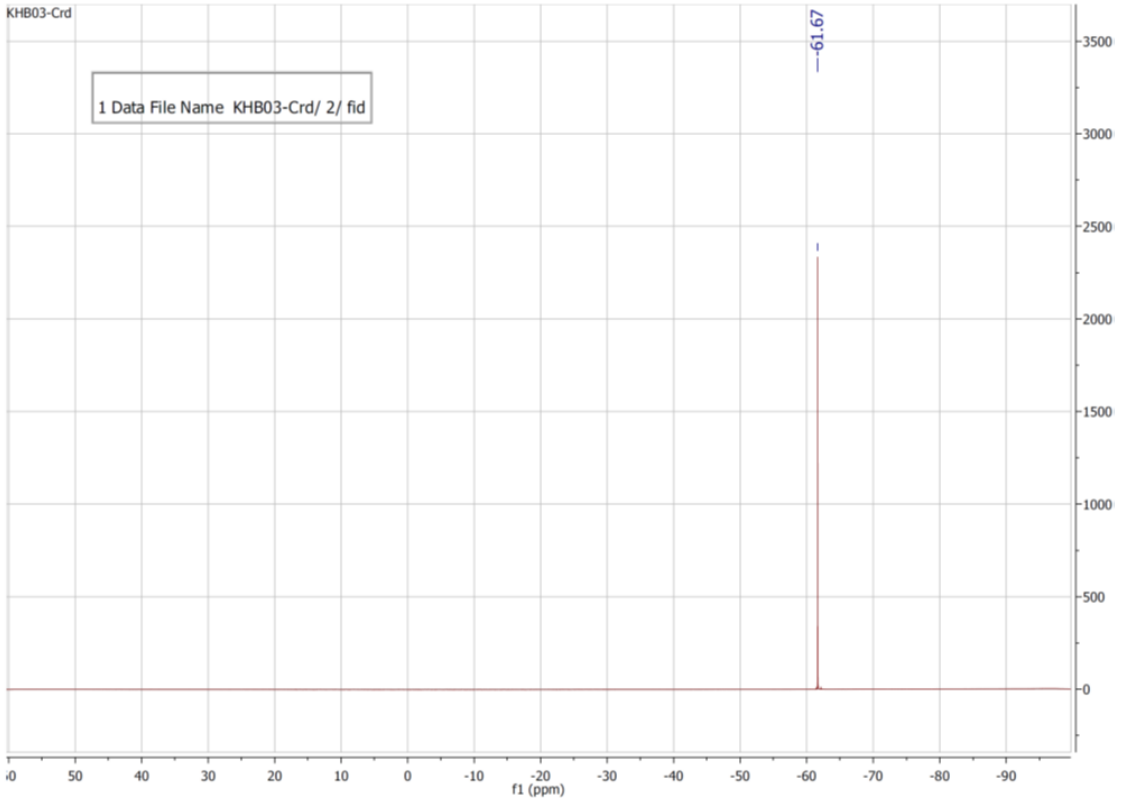

Figure **S4**. ^{19}F NMR spectrum of **L2 (CF_3-gpy)** in $CDCl_3$ at 400 MHz at r.t.

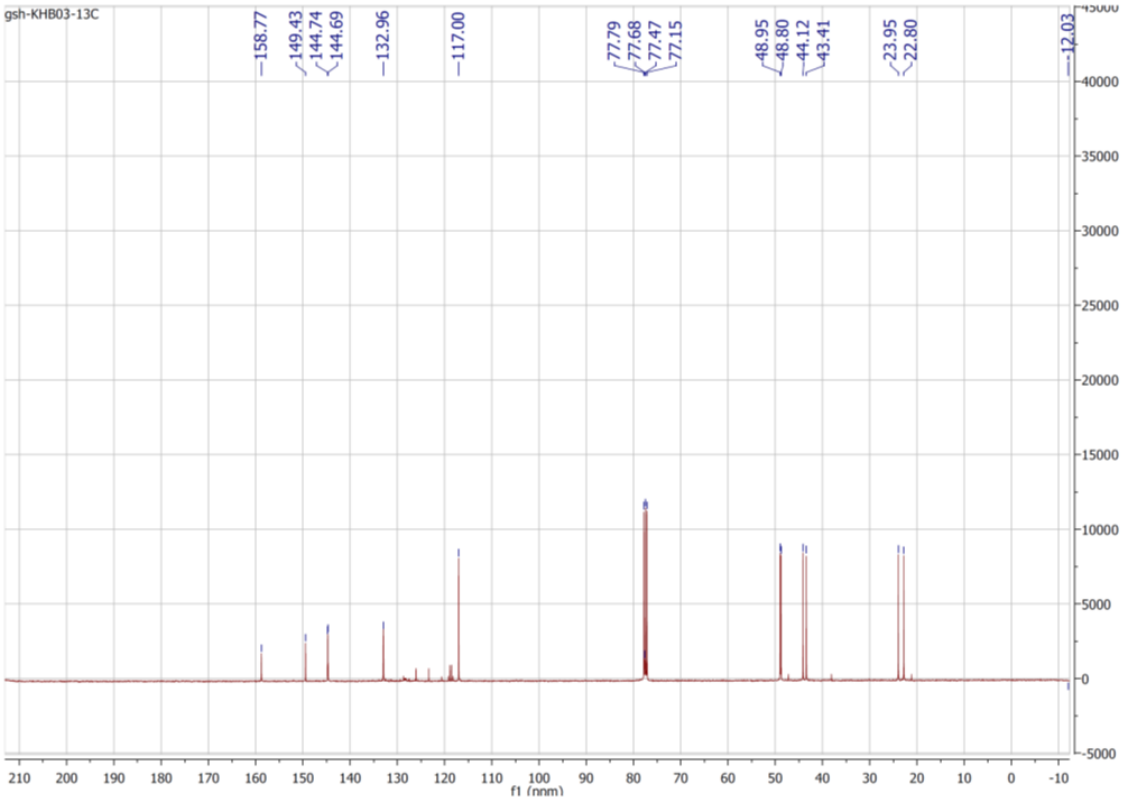

Figure **S5**. ^{13}C NMR spectrum of **L2 (CF_3-gpy)** in $CDCl_3$ at 400 MHz at r.t.

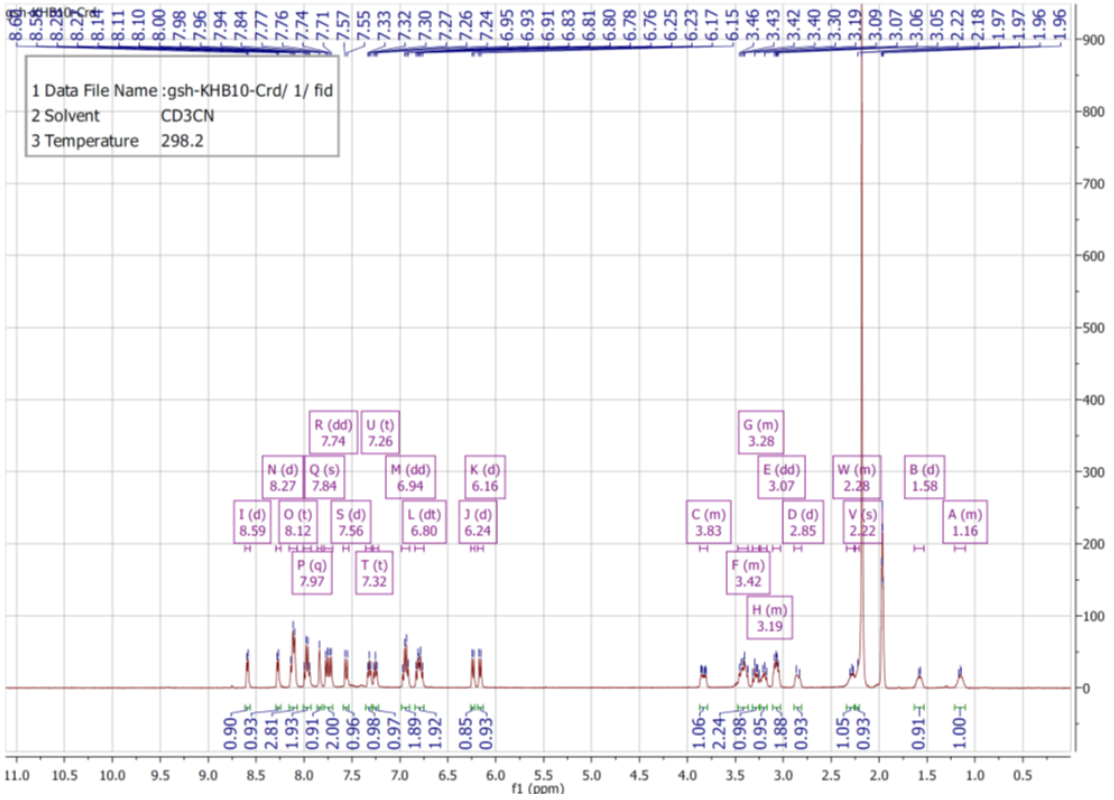

Figure **S6**. ^{1}H NMR spectrum of **[Ir(ppy)$_2$(CF_3-gpy)]PF_6, 1a** in Acetonitrile-d_3 at 400 MHz.

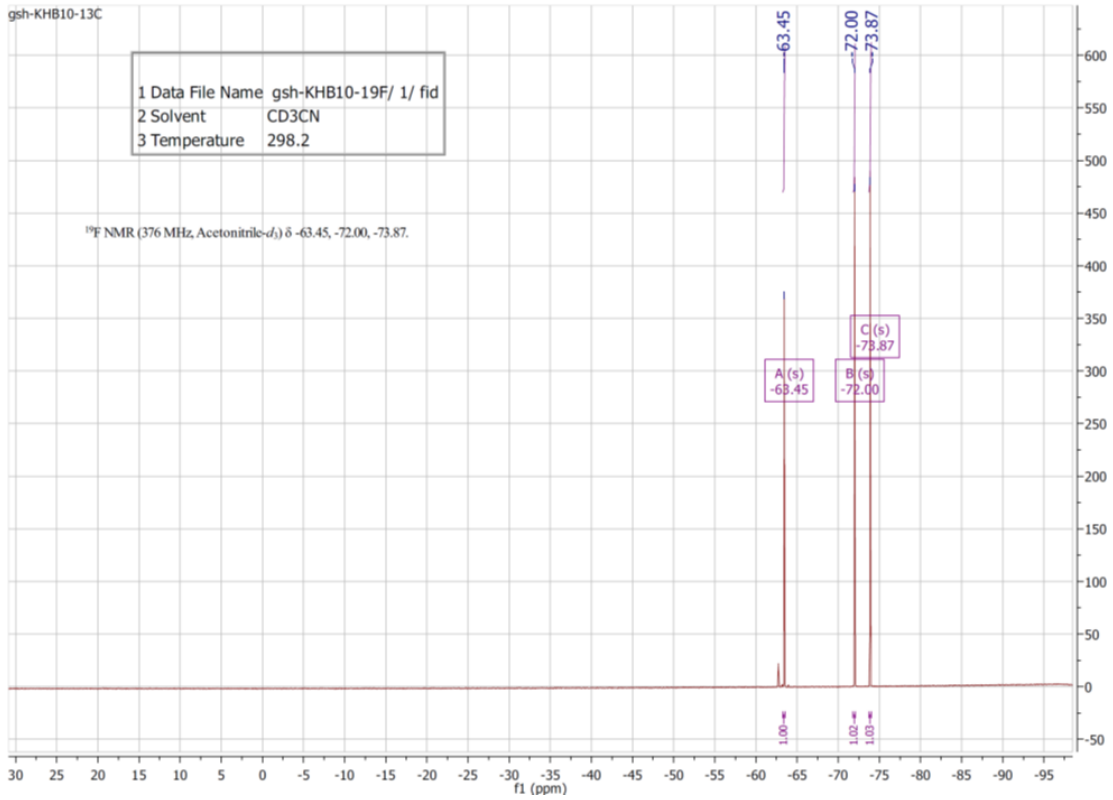

Figure **S7**. ^{19}F NMR spectrum of **[Ir(ppy)$_2$(CF$_3$-gpy)]PF$_6$, 1a** in Acetonitrile-d_3 at 400 MHz.

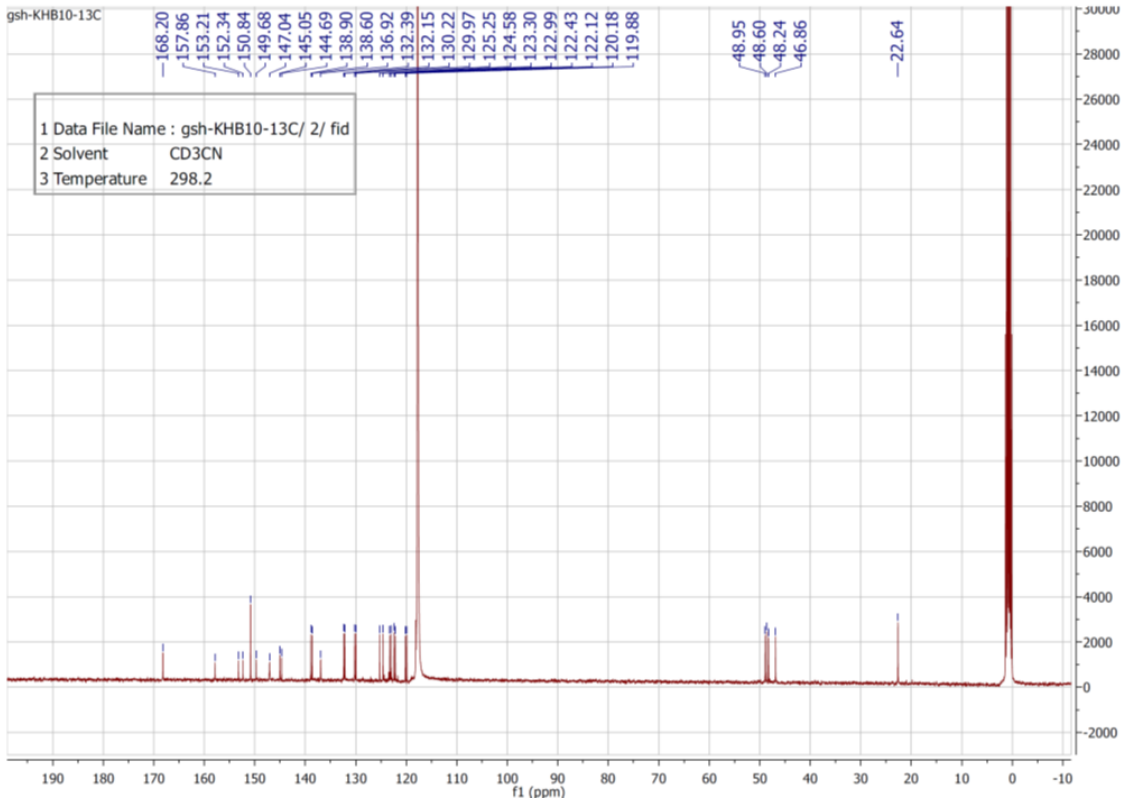

Figure **S8**. ^{13}C NMR spectrum of **[Ir(ppy)$_2$(CF$_3$-gpy)]PF$_6$, 1a** in Acetonitrile-d_3 at 400 MHz.

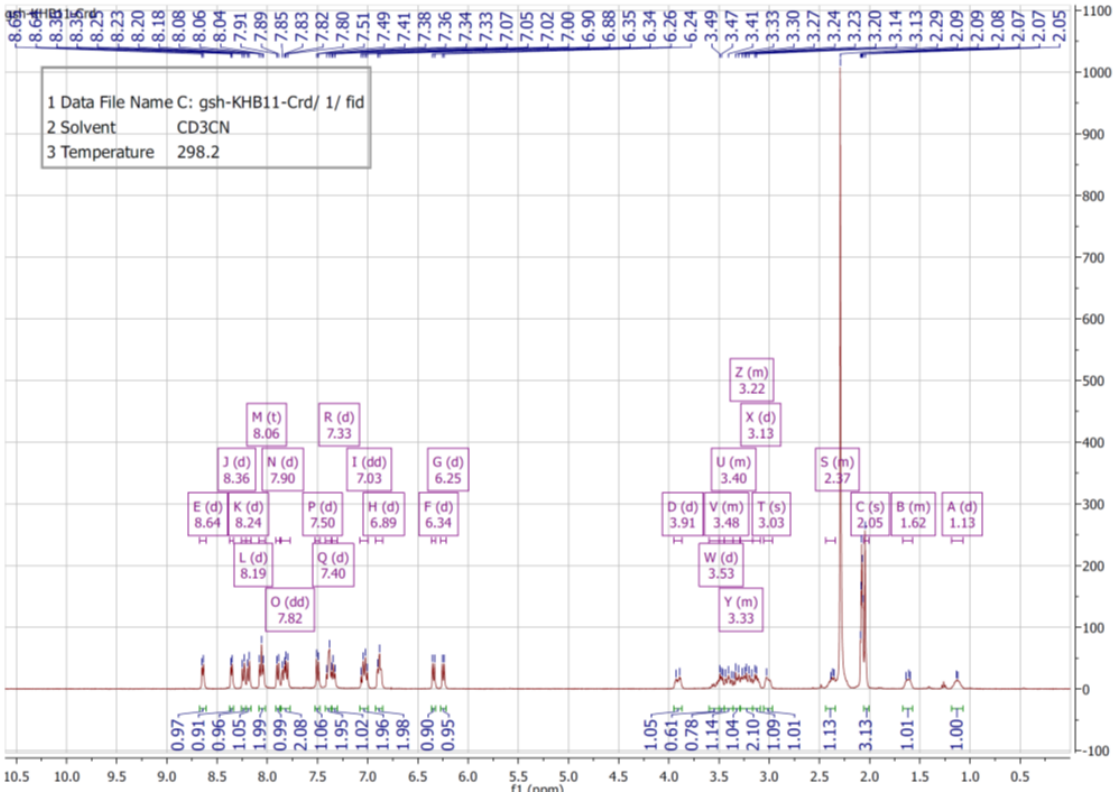

Figure **S9**. ^{1}H NMR spectrum of **[Ir(ppy)$_2$(Me-gpy)]PF$_6$, 1b** in Acetonitrile-d_3 at 400 MHz.

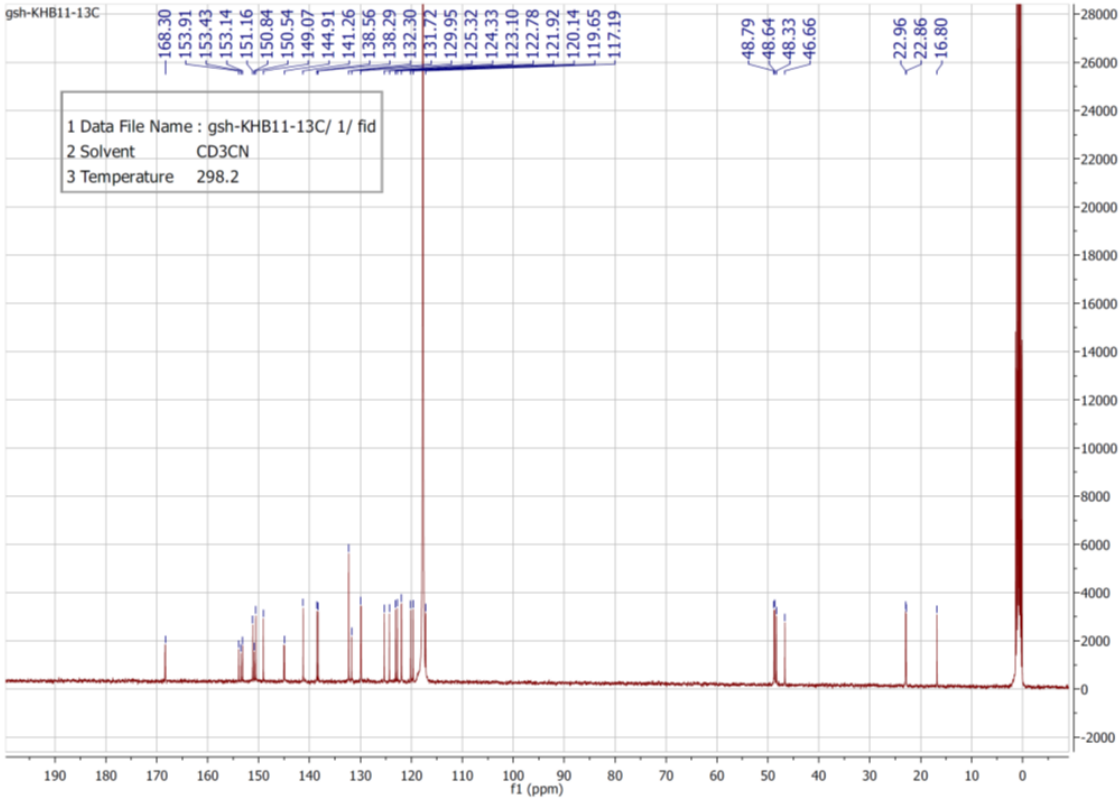

Figure **S10**. ^{13}C NMR spectrum of **[Ir(ppy)$_2$(Me-gpy)]PF$_6$, 1b** in Acetonitrile-d_3 at 400 MHz.

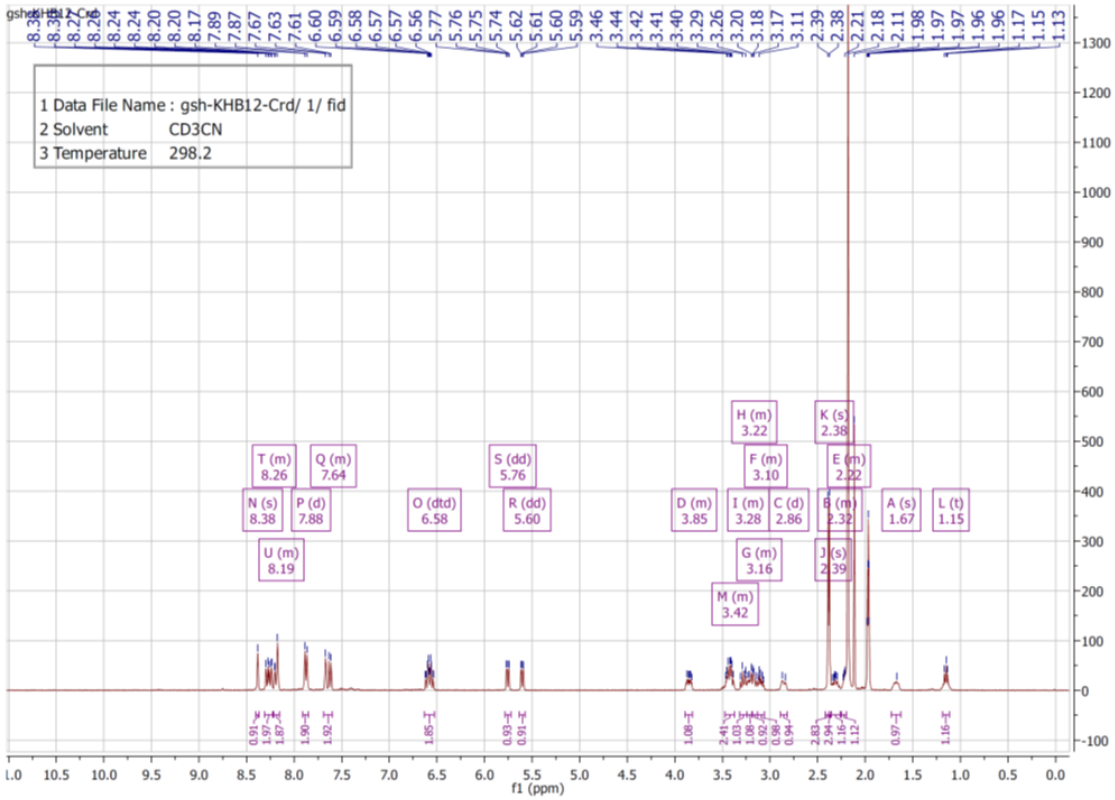

Figure **S11**. ^{1}H NMR spectrum of **[Ir(dFMeppy)$_2$(CF$_3$-gpy)]PF$_6$, 2a** in Acetonitrile-d_3 at 400 MHz.

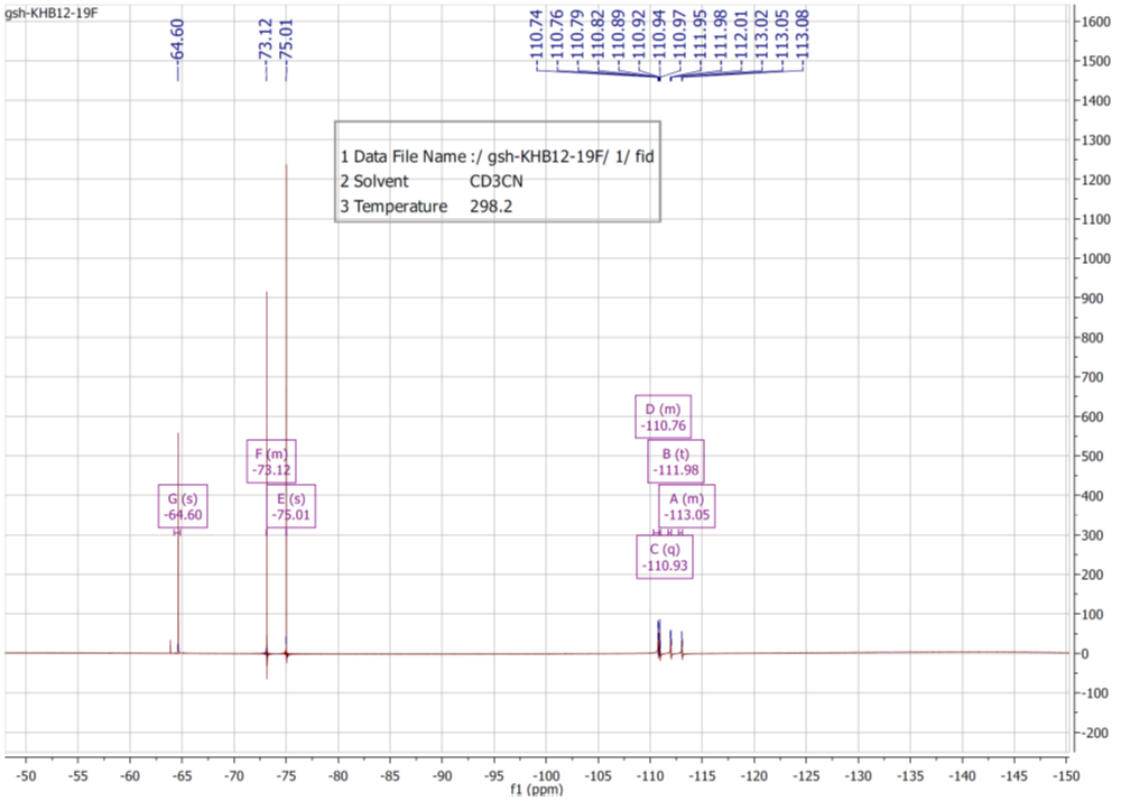

Figure **S12**. ^{19}F NMR spectrum of **[Ir(dFMeppy)$_2$(CF$_3$-gpy)]PF$_6$, 2a** in Acetonitrile-d_3 at 400 MHz.

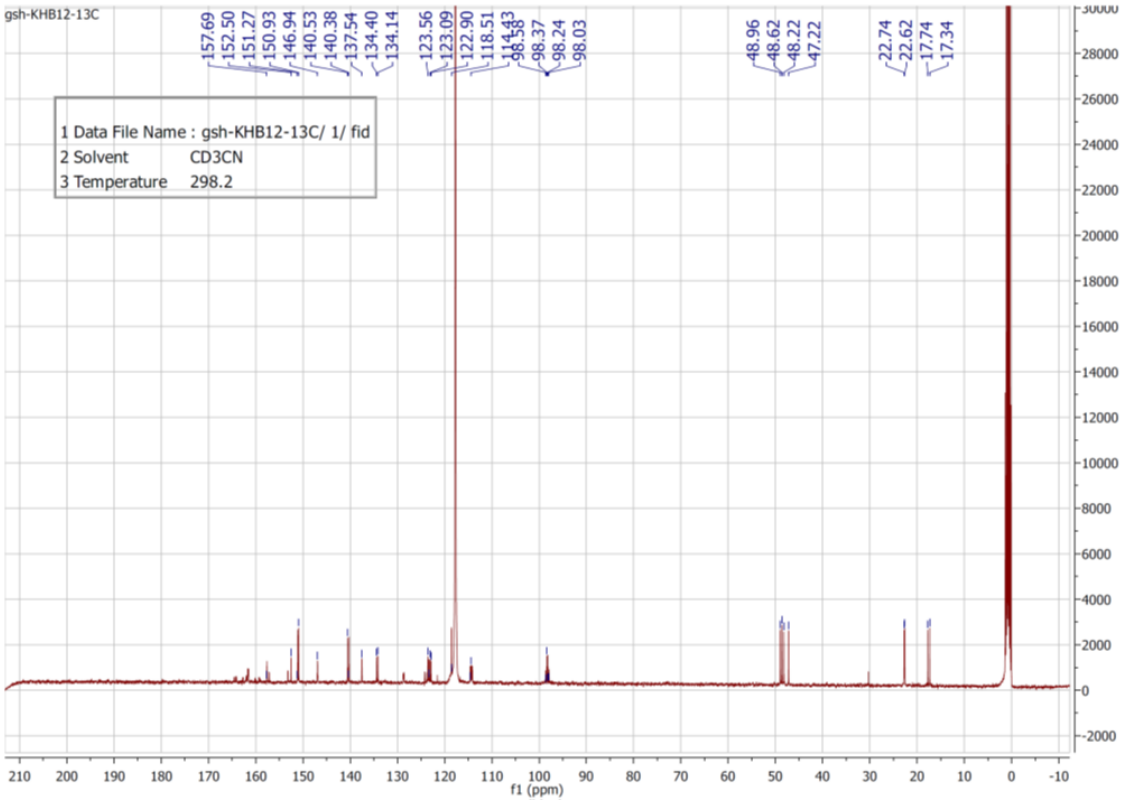

Figure **S13**. ^{13}C NMR spectrum of **[Ir(dFMeppy)$_2$(CF$_3$-gpy)]PF$_6$, 2a** in Acetonitrile-d_3 at 400 MHz.

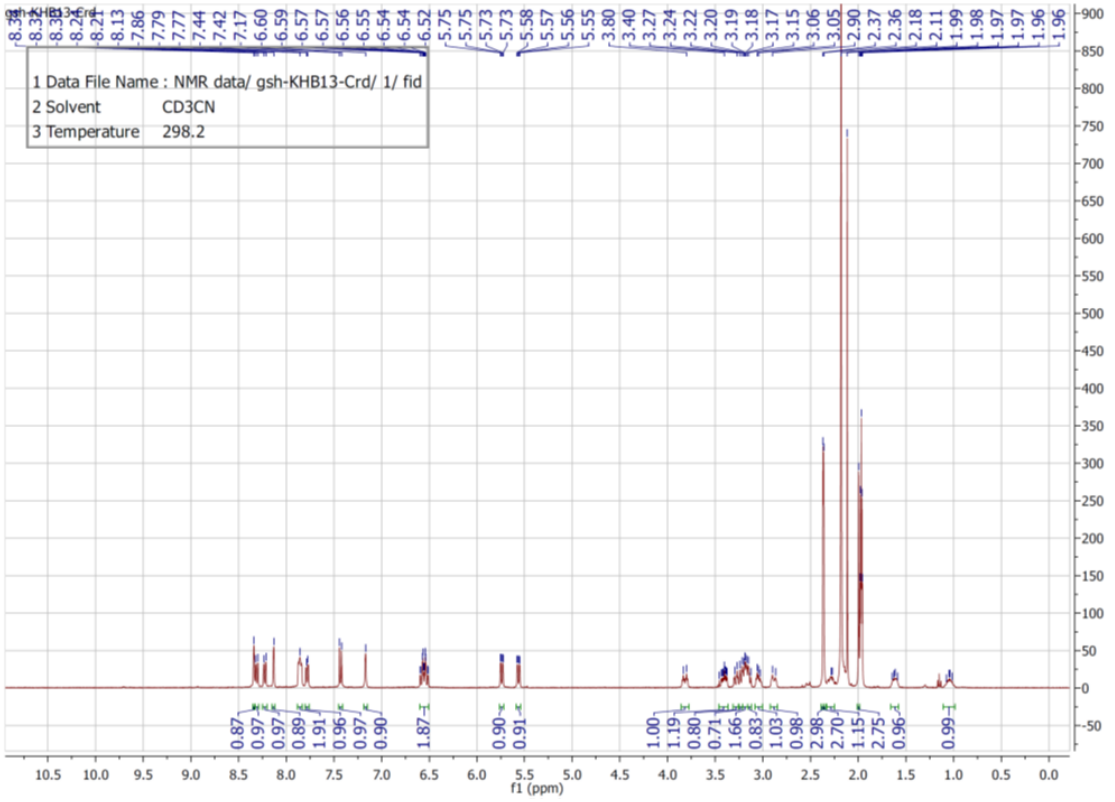

Figure **S14**. ^{1}H NMR spectrum of **[Ir(dFMeppy)$_2$(Me-gpy)]PF$_6$, 2b** in Acetonitrile-d_3 at 400 MHz.

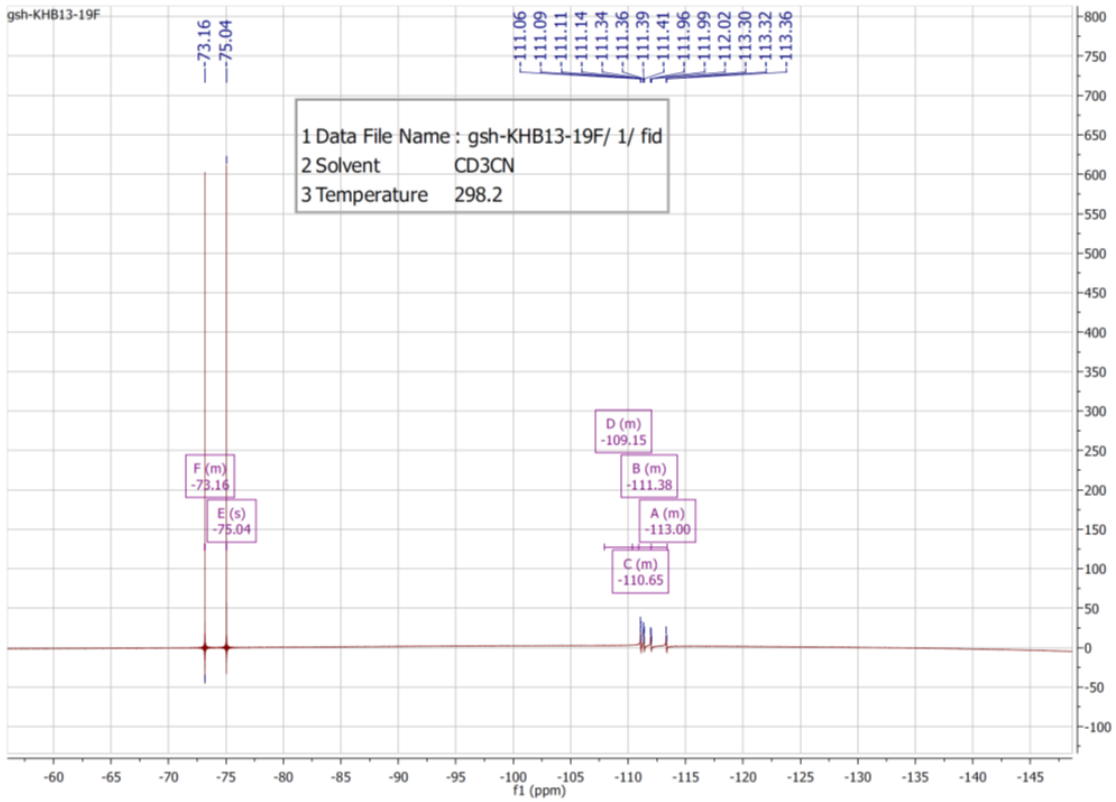

Figure **S15**. ^{19}F NMR spectrum of **[Ir(dFMeppy)$_2$(Me-gpy)]PF$_6$, 2b** in Acetonitrile-d_3 at 400 MHz.

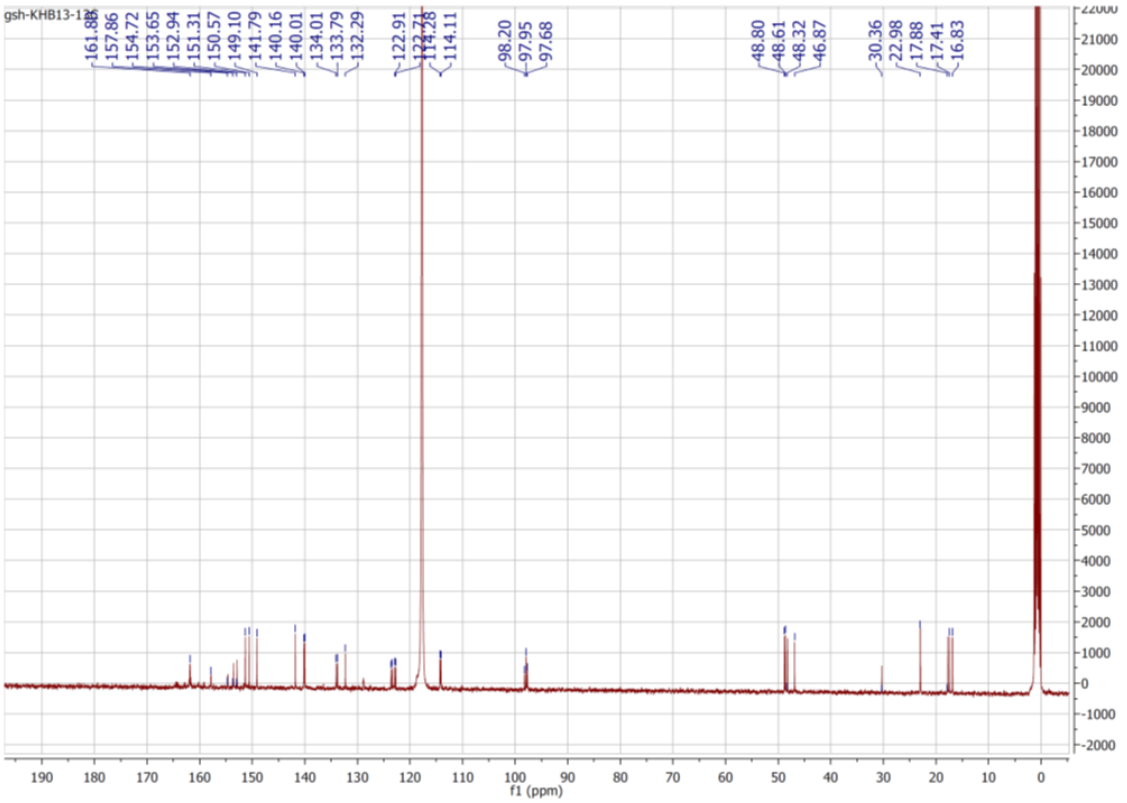

Figure **S16**. ^{13}C NMR spectrum of **[Ir(dFMeppy)$_2$(Me-gpy)]PF$_6$, 2b** in Acetonitrile-d_3 at 400 MHz at r.t.

Photophysical Characterisation

Aerated and Degassed Solution

The photophysical properties of the complexes **1a**–**2b** in aerated and degassed MeCN solution were investigated using steady-state techniques by measuring UV-Vis absorption spectra, photoluminescence (PL) spectra, PL quantum yields (Φ_{PL}), and time-resolved PL spectra using Time Correlated Single Photon Counting (TCSPC).

A Cary 300-UV-Vis spectrophotometer was used to obtain the absorption spectra of samples in the wavelength range of 200 - 800 nm. The absorbance of the samples was adjusted to be close to 0.1 at 360 nm for all investigated complexes. The PL spectra were obtained at an excitation wavelength of 360 nm using an Edinburgh instruments FLS980 fluorimeter. Solution photoluminescence quantum yield (Φ_{PL}) was measured using the optically dilute method described by Demas and Crosby[1] $\Phi_{PL}(x) = \Phi_{PL}(r)\left(\frac{A_r(\lambda_r)}{A_x(\lambda_x)}\right)\left(\frac{I(\lambda_r)}{I(\lambda_x)}\right)\left(\frac{n_x}{n_r}\right)^2\left(\frac{D_x}{D_r}\right)$, where $A(\lambda)$ is absorbance at excitation wavelength of 360 nm, $I(\lambda)$ is relative intensity of exciting light, n is the refractive index of the solvents and D is the integrated area under the corrected emission spectra (at an excitation wavelength of 360 nm). Here *x* and *r* refer to unknown and reference solutions, respectively. For Φ_{PL} measurements, the solutions were prepared by mixing complexes in MeCN (n = 1.344), whereas the reference solution was prepared by diluting quinine sulfate dihydrate in 0.5M H_2SO_4 (n = 1.35). Φ_{PL} of 54.6% was used for reference solution.[2] For lifetime measurements, the sample was excited with a 375 nm PicoQuant picosecond laser and PL emission was detected at a detection wavelength of 512 nm for **1a**, **1b** and 470 nm for **2a**, **2b**.

PL decay traces in aerated solution are given in **Fig. 2(b)** (main manuscript). The PL decays were fitted with a single exponential decay and resulting lifetimes are given in Table **1** (main manuscript). The radiative (k_r) and non-radiative decay (k_{nr}) rate constants calculated using **eq. S1** and **S2** are also given in Table **1** (main manuscript)

$$k_r = \frac{\Phi_{PL}}{\tau} \qquad (S1)$$

$$k_{nr} = \frac{(1-\Phi_{PL})}{\tau} \qquad (S2)$$

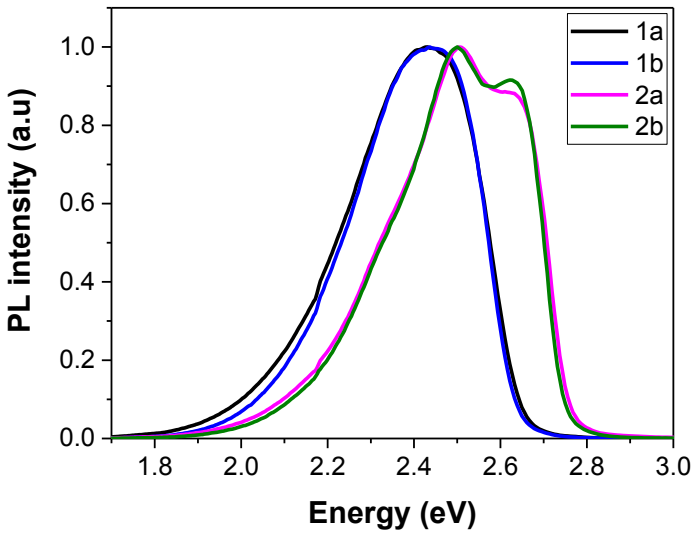

Figure S18: Emission spectra of MeCN degassed solutions, following excitation at 360 nm.

The PL spectra of degassed solutions are shown in **Fig. S18**. The PL spectra are qualitatively similar to aerated solution except with increased PL intensity in degassed solution. Huang Rhys factors were estimated by taking the ratio of the (0, 1) and (0, 0) peaks. PL decays of **1b** and **2b** in degassed solution follow mono-exponential decay whereas PL decays of **1a** and **2a** have biexponential decays (**Fig. 3**). The details about the fitting parameters are given in Table **S1**.

Table S1: The fitting parameters for time-resolved luminescence of complexes measured in degassed MeCN solution.

Materials	A_1	$\tau_1(\mu s)$	A_2	$\tau_2(\mu s)$
1a	0.87	0.09	0.13	1.60
1b	1.0	1.90	-	-
2a	0.93	0.11	0.07	0.98
2b	1.0	2.60	-	-

Solid-state thin film

We measured the PL lifetime of 2 wt% of the complexes doped into 98 wt% PMMA as thin films at different temperatures and in different environments (air, vacuum). Table **S2** shows the fitted lifetime parameters.

Table S2: The fitting parameters for time-resolved luminescence of 2wt% of **2a** in PMMA (**Fig. 6(b)**) at various temperatures.

Environment	A_1	$\tau_1(\mu s)$	A_2	$\tau_2(\mu s)$
RT-air	0.09	0.82	0.91	2.80
RT-vacuum	0.10	0.92	0.90	3.00
150K-vacuum	1.0	3.20	-	-
77K-vacuum	1.0	3.70	-	-

In conjunction with transient PL measurements, we measured the Φ_{PL} of complexes **2a** and **2b** in air and under N_2. For films, Φ_{PL} was measured using an integrating sphere and excitation wavelength of 380 nm and the results are compared with solution in Table **S3**. The Φ_{PL} of **2a** increased by more than 30 times compared to degassed solution and increases even further when measured under N_2. In the case of **2b**, Φ_{PL} also increases on going from solution to film, but by a much smaller amount.

Table S3: Comparison of $\boldsymbol{\Phi_{PL}}$ values of solution (before degassing, after degassing) and solid-state films (in air and under N_2) of **2a** and **2b**. For solution, an excitation wavelength of 360 nm was used and for solid-state, an excitation wavelength of 380 nm was used.

Materials	PLQY(%) Solution Before degassing	PLQY(%) Solution, after degassing	PLQY(%) Film RT-Air	PLQY(%) Film RT-N_2
2a	1.0	1.7	65.9	72.4
2b	1.2	65.6	82.7	88.6

DFT Calculations:

Computational details:

All calculations were performed with the Gaussian09, revision D.01[3] suite of programs employing the DFT method, the Becke three-parameter hybrid functional,[4] and Lee-Yang-Parr's gradient-corrected correlation functional (B3LYP).[5] Singlet and triplet ground state geometry optimizations for [**1a**]$^+$, [**1b**]$^+$, [**2a**]$^+$ and [**2b**]$^+$ were carried out at the (R)B3LYP and (U)B3LYP levels in the gas phase, using their respective crystallographic structures as starting points. All elements except Iridium were assigned the 6-31G(d,p) basis set.[6]The double- ζ quality SBKJC VDZ ECP basis set[7] with an effective core potential was employed for the Ir(III)-ion. Vibrational frequency calculations were performed to ensure that the optimized geometries represent the local minima and there are only positive eigenvalues, except frequency mode no. 1 for **1a** and **2a**, which were found to be rotational motion of the $-CF_3$ group around the C-C bond of the pyridine ring of the guanidylpyridine (gpy) unit. The electronic distribution and localization of the singlet excited states were visualized using the electron density difference maps (ED-DMs).[8] *Gausssum 2.2* and *Chemissian* were employed to visualize the absorption spectra (simulated with Gaussian distribution with a full-width at half maximum (fwhm) set to 3000 cm^{-1}) and to calculate the fractional contributions of various groups to each molecular orbital. All calculated structures and Kohn-Sham orbitals were visualized with ChemCraft.[9]

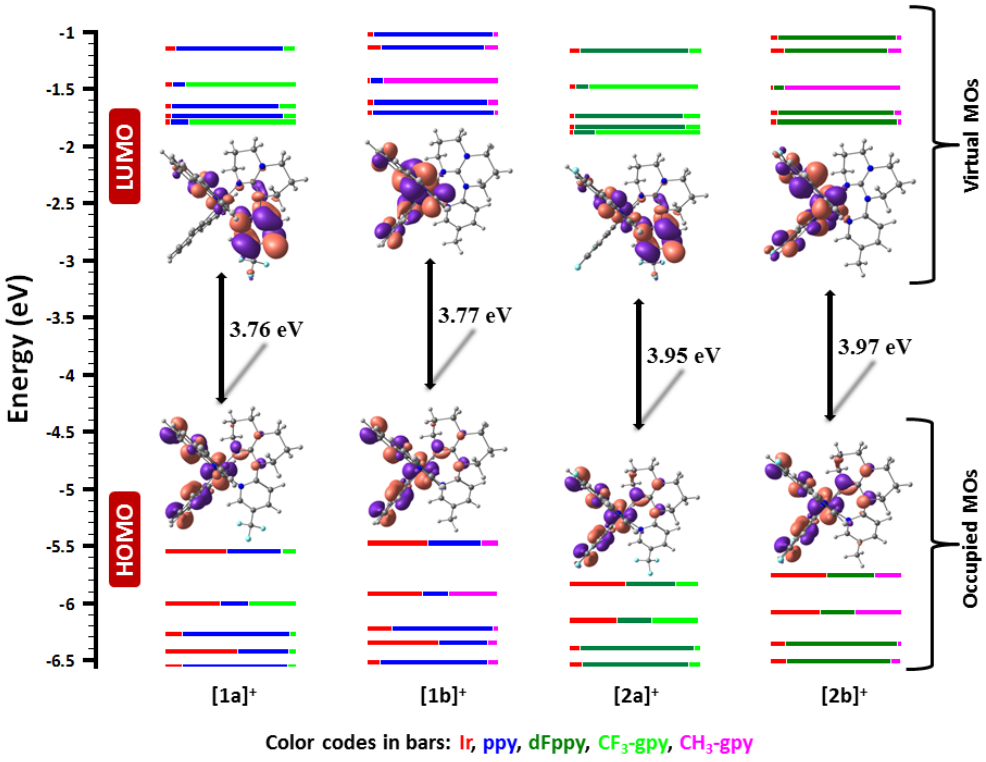

Figure S20: Calculated frontier MO energies of [**1a**]$^+$, [**1b**]$^+$, [**2a**]$^+$ and [**2b**]$^+$, obtained from DFT [(B3LYP/SBKJC-VDZ for Ir(III)) and (6-31g** for C,H,N,F] with CPCM(CH_3CN) and 0.5 eV threshold of degeneracy (orbitals are isocontoured at 0.03). Kohn-Sham MOs of [**1a**]$^+$, [**1b**]$^+$, [**2a**]$^+$ and [**2b**]$^+$ are also shown.

Table S4. Vibrational modes and their associated energies contributing to deactivation in complex **2a** but less in complex **2b**.

Vibrational mode no.	Status	Energy associated (cm^{-1})	Nature of the mode
115	Present in **2a** but absent in **2b**	1029.62	Symmetric stretching of the C-C and C-N bonds in pyridine part of C^N ligand couples with wagging mode of C and N atoms of the pyridine ring of the gpy ligand
121	Strongly present in **2a** but very weakly present in **2b**	1054.21 (for **2a**) 1090.90 (for **2b**)	Asymmetric stretching modes of the Ir-N_{dFppy} bonds couple with the asymmetric stretching modes of the C-N and C-C bonds of the pyriding ring of the gpy ligand
148	Present in **2a** but very weakly present in **2b**	1293.30 (for **2a**) 1315.06 (for **2b**)	Asymmetric stretching modes of the Ir-C_{dFppy} bonds couple with the asymmetric stretching modes of the C-N and C-C bonds of the pyriding ring of the gpy ligand
149	Present in **2a** but absent in **2b**	1294.48	Asymmetric stretching modes of the Ir-C_{dFppy} bonds couple with the asymmetric stretching modes of the C-N and C-C bonds of the pyriding ring of the gpy ligand
151	Present in **2a** but absent in **2b**	1311.82	Assymmetric wagging modes of the Ir-N_{dFppy} bonds couple with the wagging mode of the C-N of the pyriding ring of the gpy ligand
153	Present in **2a** but very weakly present in **2b**	1317.10 (for **2a**) 1340.73 (for **2b**)	Assymmetric wagging modes of the Ir-N_{dFppy} bonds couple with the rocking mode of the C-N bonds of the pyriding ring of the gpy ligand
169	Present in **2a** but absent in **2b**	1450.11	Assymmetric stretching modes of C-C bonds in phenyl part of the C^N ligand couple with rocking mode of the C-H bond adjacent to pyridine N-atom of the gpy ligand.

Table S5. Optimized Atomic coordinates obtained from DFT calculations of [**1a**]$^{+}$

Center Number	Atomic Number	Atomic Type	Coordinates (Angstroms) X	Y	Z
1	77	0	-0.299272	-0.503853	-0.031980
2	7	0	0.913081	-1.211374	-1.582674
3	7	0	-1.526542	-0.059153	1.598792
4	7	0	1.172939	1.161529	0.225251
5	6	0	3.147761	3.137383	0.194210
6	7	0	-0.540387	2.823468	0.083045
7	7	0	-2.500112	3.116895	-1.184572
8	7	0	-1.334831	1.065618	-1.265838
9	6	0	0.754321	-1.927677	0.965511
10	6	0	1.665614	-2.661658	0.156266
11	6	0	2.462984	-3.685094	0.700409
12	1	0	3.157746	-4.238774	0.075782
13	6	0	2.369384	-3.997542	2.050584
14	1	0	2.983249	-4.787238	2.471550
15	6	0	1.477979	-3.285347	2.860537
16	1	0	1.399294	-3.527708	3.917002
17	6	0	0.683603	-2.269890	2.324568
18	1	0	-0.004808	-1.747880	2.981926
19	6	0	1.728286	-2.260750	-1.248485
20	6	0	0.930157	-0.723103	-2.839741
21	1	0	0.279722	0.122174	-3.021608
22	6	0	1.726676	-1.257657	-3.840102
23	1	0	1.701150	-0.831911	-4.836581
24	6	0	2.546803	-2.345781	-3.526282
25	1	0	3.179881	-2.797207	-4.283655
26	6	0	2.548230	-2.839901	-2.230238
27	1	0	3.183677	-3.676607	-1.967159
28	6	0	-1.768675	-1.870010	-0.311825
29	6	0	-2.852851	-1.768379	0.602287
30	6	0	-3.979954	-2.601327	0.489519
31	1	0	-4.805961	-2.514777	1.189554
32	6	0	-4.045208	-3.553866	-0.520369
33	1	0	-4.913651	-4.199000	-0.606296
34	6	0	-2.978182	-3.679566	-1.416223
35	1	0	-3.018412	-4.431491	-2.199814
36	6	0	-1.858239	-2.851064	-1.311118
37	1	0	-1.046124	-2.978706	-2.020530
38	6	0	-2.688828	-0.778966	1.664623
39	6	0	-1.228198	0.818536	2.577693
40	1	0	-0.270546	1.314903	2.487538

41	6	0	-2.072821	1.064559	3.649177
42	1	0	-1.781239	1.773091	4.416116
43	6	0	-3.283807	0.367277	3.713881
44	1	0	-3.973273	0.532071	4.535927
45	6	0	-3.584606	-0.555602	2.723320
46	1	0	-4.505249	-1.124434	2.770868
47	6	0	0.826841	2.463124	0.104359
48	6	0	1.807424	3.469303	0.066864
49	1	0	1.520621	4.502190	-0.083968
50	6	0	3.493015	1.794231	0.343212
51	6	0	4.925424	1.365843	0.543636
52	6	0	2.478870	0.846560	0.335453
53	1	0	2.701165	-0.208929	0.435469
54	6	0	-0.944552	4.050635	0.795483
55	1	0	-0.119832	4.367345	1.432624
56	1	0	-1.785085	3.801303	1.454895
57	6	0	-1.354928	5.114057	-0.214459
58	1	0	-1.625148	6.052507	0.278184
59	1	0	-0.520119	5.325324	-0.891045
60	6	0	-2.556663	4.572869	-0.980864
61	1	0	-3.476440	4.786152	-0.420522
62	1	0	-2.659122	5.061550	-1.958254
63	6	0	-3.705963	2.597037	-1.858245
64	1	0	-3.769811	3.075152	-2.844636
65	1	0	-4.581682	2.925283	-1.284194
66	6	0	-3.675361	1.082056	-2.005235
67	1	0	-4.380674	0.776546	-2.783645
68	1	0	-3.973347	0.586768	-1.076193
69	6	0	-2.246952	0.672898	-2.350966
70	1	0	-2.168745	-0.404400	-2.489281
71	1	0	-1.942492	1.158507	-3.290736
72	6	0	-1.470573	2.290092	-0.825926
73	1	0	3.914337	3.903501	0.156200
74	9	0	5.776687	2.265072	0.013789
75	9	0	5.216947	1.248687	1.853581
76	9	0	5.161232	0.170996	-0.032945

Table S6. Optimized Atomic coordinates obtained from DFT calculations of [**1b**]$^{+}$

Center Number	Atomic Number	Atomic Type	Coordinates (Angstroms) X	Y	Z
1	77	0	0.379026	-0.180801	0.000920
2	7	0	1.684968	0.623467	-1.419849
3	7	0	-0.720280	-1.154964	1.483910
4	7	0	-0.197472	1.919051	0.514309
5	6	0	-0.736992	4.640390	0.739824
6	7	0	-2.524730	1.434885	0.220148
7	7	0	-3.814309	0.113446	-1.235787
8	7	0	-1.456714	-0.015041	-1.287898
9	6	0	2.117597	-0.227007	1.052760
10	6	0	3.259459	0.207161	0.323006
11	6	0	4.538084	0.221928	0.909524
12	1	0	5.404232	0.554390	0.344616
13	6	0	4.706009	-0.191160	2.225129
14	1	0	5.692199	-0.182301	2.678184
15	6	0	3.593380	-0.618892	2.958170
16	1	0	3.719716	-0.944996	3.987205
17	6	0	2.323216	-0.637863	2.379035
18	1	0	1.485715	-0.987084	2.974787
19	6	0	3.001689	0.659098	-1.043446
20	6	0	1.322115	1.076165	-2.636881
21	1	0	0.261374	1.044721	-2.848860
22	6	0	2.237792	1.556086	-3.560404
23	1	0	1.896869	1.903989	-4.528749
24	6	0	3.590741	1.571907	-3.208124
25	1	0	4.339562	1.930900	-3.907244
26	6	0	3.967091	1.129016	-1.948434
27	1	0	5.009790	1.142616	-1.655271
28	6	0	0.713391	-2.111650	-0.520330
29	6	0	0.013946	-3.066766	0.267144
30	6	0	0.097923	-4.442416	-0.011463
31	1	0	-0.442978	-5.165035	0.592950
32	6	0	0.883324	-4.894215	-1.065295
33	1	0	0.950725	-5.956039	-1.279374
34	6	0	1.592248	-3.969085	-1.838908
35	1	0	2.217980	-4.317465	-2.656376
36	6	0	1.508337	-2.601221	-1.568034
37	1	0	2.077428	-1.912259	-2.184852
38	6	0	-0.753421	-2.519599	1.383721
39	6	0	-1.327672	-0.546013	2.522029
40	1	0	-1.223386	0.530751	2.559865
41	6	0	-2.028294	-1.242014	3.495265
42	1	0	-2.490988	-0.705746	4.316005
43	6	0	-2.102106	-2.635097	3.392434
44	1	0	-2.640994	-3.216548	4.133955
45	6	0	-1.460405	-3.268614	2.338667
46	1	0	-1.486051	-4.348280	2.255010
47	6	0	-1.462957	2.364380	0.379016
48	6	0	-1.751758	3.735139	0.466577
49	1	0	-2.763310	4.088160	0.307000
50	6	0	0.575940	4.185239	0.915449

51	6	0	1.714650	5.117915	1.236083
52	6	0	0.780601	2.815853	0.770362
53	1	0	1.773039	2.393777	0.879672
54	6	0	-3.784624	1.695306	0.939422
55	1	0	-3.608904	2.490246	1.663068
56	1	0	-4.054273	0.794820	1.505977
57	6	0	-4.879589	2.041701	-0.061352
58	1	0	-5.822493	2.279184	0.439751
59	1	0	-4.583360	2.920592	-0.643585
60	6	0	-5.070557	0.827974	-0.963636
61	1	0	-5.753306	0.115348	-0.481761
62	1	0	-5.529277	1.109947	-1.920164
63	6	0	-4.020048	-1.093336	-2.058679
64	1	0	-4.439363	-0.774061	-3.022175
65	1	0	-4.780816	-1.713403	-1.567415
66	6	0	-2.728034	-1.868783	-2.274630
67	1	0	-2.839409	-2.531521	-3.137954
68	1	0	-2.489630	-2.492154	-1.407572
69	6	0	-1.603737	-0.858889	-2.483584
70	1	0	-0.655522	-1.361897	-2.667283
71	1	0	-1.830183	-0.232455	-3.360124
72	6	0	-2.568306	0.483430	-0.806102
73	1	0	-0.964039	5.700920	0.805628
74	1	0	1.803953	5.905753	0.480675
75	1	0	1.559670	5.610513	2.202032
76	1	0	2.666613	4.583962	1.281820

Table S7. Optimized Atomic coordinates obtained from DFT calculations of [**2a**]$^{+}$

Center Number	Atomic Number	Atomic Type	Coordinates (Angstroms) X	Y	Z
1	77	0	-0.264059	-0.177326	-0.088916
2	7	0	0.819579	-0.951519	-1.701762
3	7	0	-1.399419	0.328538	1.589484
4	7	0	1.401591	1.277765	0.189734
5	6	0	3.601406	2.999656	0.171194
6	7	0	-0.098087	3.138522	0.175821
7	7	0	-2.035698	3.727235	-1.019189
8	7	0	-1.143876	1.549775	-1.211228
9	6	0	0.637346	-1.755701	0.817518
10	6	0	1.423136	-2.562720	-0.060843
11	6	0	2.072270	-3.694440	0.464814
12	9	0	2.823521	-4.481819	-0.336582
13	6	0	1.988333	-4.058426	1.797497
14	1	0	2.500807	-4.935464	2.171668
15	6	0	1.218669	-3.248108	2.626209
16	9	0	1.119172	-3.576418	3.923619
17	6	0	0.548569	-2.118649	2.165397
18	1	0	-0.041718	-1.551914	2.875412
19	6	0	1.504713	-2.113581	-1.449359
20	6	0	0.861865	-0.397954	-2.930415
21	1	0	0.319305	0.531392	-3.042139
22	6	0	1.552894	-0.969946	-3.986549

23	1	0	1.552527	-0.488095	-4.957463
24	6	0	2.233293	-2.168633	-3.758764
25	1	0	2.780049	-2.654531	-4.560709
26	6	0	2.214145	-2.735773	-2.492134
27	1	0	2.743270	-3.655253	-2.293007
28	6	0	-1.882847	-1.355061	-0.388832
29	6	0	-2.928602	-1.169432	0.564562
30	6	0	-4.120306	-1.897768	0.406824
31	9	0	-5.138763	-1.733658	1.281384
32	6	0	-4.322776	-2.796642	-0.626530
33	1	0	-5.251599	-3.344917	-0.718826
34	6	0	-3.277050	-2.966220	-1.528271
35	9	0	-3.441190	-3.835226	-2.537538
36	6	0	-2.075819	-2.268912	-1.430468
37	1	0	-1.310284	-2.465268	-2.171797
38	6	0	-2.637511	-0.254805	1.665139
39	6	0	-0.970283	1.123493	2.589769
40	1	0	0.035526	1.508885	2.483440
41	6	0	-1.745721	1.420225	3.699603
42	1	0	-1.349134	2.055955	4.483027
43	6	0	-3.026522	0.866206	3.777090
44	1	0	-3.667760	1.073365	4.628048
45	6	0	-3.469725	0.028607	2.763527
46	1	0	-4.446542	-0.428041	2.814529
47	6	0	1.214114	2.614839	0.133900
48	6	0	2.309797	3.496174	0.102654
49	1	0	2.146416	4.561465	0.002267
50	6	0	3.784175	1.618197	0.257851
51	6	0	5.166232	1.028104	0.391216
52	6	0	2.663555	0.802405	0.244913
53	1	0	2.761757	-0.274351	0.293183
54	6	0	-0.324662	4.375823	0.948446
55	1	0	0.549871	4.559104	1.571213
56	1	0	-1.172159	4.205751	1.623828
57	6	0	-0.624290	5.523950	-0.005777
58	1	0	-0.761898	6.466511	0.531732
59	1	0	0.211834	5.659179	-0.699928
60	6	0	-1.904253	5.169475	-0.754037
61	1	0	-2.774891	5.468629	-0.155985
62	1	0	-1.971734	5.709003	-1.707128
63	6	0	-3.311659	3.393619	-1.682302
64	1	0	-3.331881	3.913664	-2.648924
65	1	0	-4.126108	3.808540	-1.075577
66	6	0	-3.479541	1.894230	-1.884116
67	1	0	-4.236199	1.711915	-2.652776
68	1	0	-3.817391	1.407093	-0.964193
69	6	0	-2.124191	1.319636	-2.284265
70	1	0	-2.187172	0.247636	-2.464846
71	1	0	-1.781204	1.798624	-3.213826
72	6	0	-1.112008	2.764309	-0.722421
73	1	0	4.453968	3.669675	0.135784
74	9	0	6.041623	1.681434	-0.397094
75	9	0	5.610507	1.127366	1.658652
76	9	0	5.180218	-0.274315	0.049924

Table S8. Optimized Atomic coordinates obtained from DFT calculations of [**2b**]$^{+}$

Center Number	Atomic Number	Atomic Type	Coordinates (Angstroms) X	Y	Z
1	77	0	-0.142633	-0.039157	-0.058060
2	7	0	-1.245020	-0.921480	-1.598399
3	7	0	0.725250	0.981067	1.542126
4	7	0	0.672426	-2.067490	0.382242
5	6	0	1.557221	-4.702149	0.534669
6	7	0	2.926410	-1.266720	0.275670
7	7	0	4.115279	0.265789	-1.052353
8	7	0	1.764762	0.119142	-1.224658
9	6	0	-1.926250	-0.281285	0.881353
10	6	0	-2.956996	-0.814274	0.047487
11	6	0	-4.238481	-1.000257	0.595802
12	9	0	-5.238155	-1.503857	-0.163329
13	6	0	-4.546564	-0.695699	1.910317
14	1	0	-5.543660	-0.850203	2.302390
15	6	0	-3.519031	-0.183097	2.696227
16	9	0	-3.788051	0.120215	3.976273
17	6	0	-2.232153	0.027904	2.211306
18	1	0	-1.495208	0.443053	2.888408
19	6	0	-2.568838	-1.151856	-1.320918
20	6	0	-0.743541	-1.246387	-2.806566
21	1	0	0.314261	-1.060665	-2.936829
22	6	0	-1.520360	-1.785547	-3.819880
23	1	0	-1.070828	-2.024887	-4.776728
24	6	0	-2.877733	-1.999227	-3.569067
25	1	0	-3.524021	-2.409471	-4.338676
26	6	0	-3.399438	-1.688635	-2.320796
27	1	0	-4.443621	-1.855506	-2.104122
28	6	0	-0.707341	1.855249	-0.499942
29	6	0	-0.183106	2.844387	0.385738
30	6	0	-0.471581	4.195982	0.130534
31	9	0	0.022883	5.161906	0.937887
32	6	0	-1.251241	4.611939	-0.935464
33	1	0	-1.457813	5.661310	-1.102687
34	6	0	-1.759975	3.621259	-1.769246
35	9	0	-2.524534	3.994038	-2.807805
36	6	0	-1.503433	2.266879	-1.574529
37	1	0	-1.941064	1.558661	-2.268249
38	6	0	0.583633	2.344428	1.523778
39	6	0	1.337216	0.383586	2.583909
40	1	0	1.370858	-0.697667	2.549428
41	6	0	1.875063	1.092937	3.646460
42	1	0	2.347899	0.564124	4.466236
43	6	0	1.772630	2.486566	3.629505
44	1	0	2.180482	3.080582	4.441350
45	6	0	1.125867	3.110198	2.572054
46	1	0	1.016122	4.183956	2.550924
47	6	0	1.992839	-2.334877	0.321907
48	6	0	2.456772	-3.658617	0.376395
49	1	0	3.515073	-3.866561	0.278935
50	6	0	0.185347	-4.433925	0.627055
51	6	0	-0.836748	-5.524557	0.817269

52	6	0	-0.191047	-3.098214	0.524337
53	1	0	-1.236770	-2.818420	0.573545
54	6	0	4.170266	-1.400623	1.055892
55	1	0	4.056934	-2.238337	1.742742
56	1	0	4.295796	-0.496363	1.664452
57	6	0	5.349672	-1.571346	0.107226
58	1	0	6.287648	-1.710221	0.652573
59	1	0	5.197007	-2.457036	-0.518411
60	6	0	5.434582	-0.308792	-0.743524
61	1	0	6.004569	0.459819	-0.205135
62	1	0	5.965310	-0.496937	-1.685544
63	6	0	4.214690	1.528962	-1.808430
64	1	0	4.712540	1.310123	-2.762254
65	1	0	4.872098	2.207444	-1.250295
66	6	0	2.850441	2.157475	-2.055332
67	1	0	2.921691	2.874521	-2.878432
68	1	0	2.500057	2.699910	-1.171772
69	6	0	1.867655	1.034505	-2.371709
70	1	0	0.875607	1.428692	-2.586683
71	1	0	2.211259	0.485239	-3.261601
72	6	0	2.904868	-0.268589	-0.705748
73	1	0	1.920420	-5.725379	0.574448
74	1	0	-0.767594	-6.272111	0.020082
75	1	0	-0.681658	-6.047230	1.767142
76	1	0	-1.853137	-5.124015	0.817313

Device Fabrication and Testing

The electrical and optical properties of EL devices using **1b**, **2a** and **2b** were investigated by fabricating OLEDs with the active layer deposited from solution. The device architecture is given in **Fig. 7** of the main text. The irradiance, current, and voltage of the device were measured under an ambient environment with a Keithley 2400 SourceMeter and 2000 Multimeter connected to a calibrated silicon photodiode. The electroluminescence spectrum was captured by an Andor DV420-BV CCD spectrometer For a comparison between PL and EL, we plotted the EL spectra against energy.

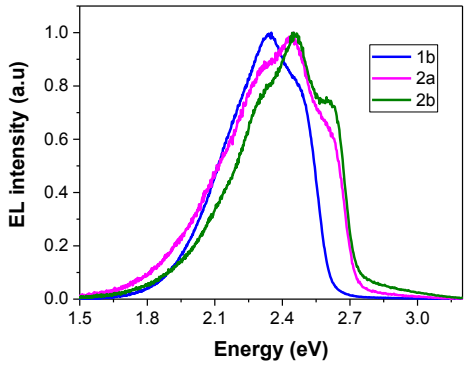

Figure S21: Electroluminescence spectra of complexes **1b**, **2a** and **2b**.

References

1. G. A. Crosby and J. N. Demas, *J. Phys. Chem.,* 1971, **75**, 991-1024.

2. W. Melhuish, *J. Phys. Chem.*, 1961, **65**, 229-235**.**
3. Gaussian 09, Revision D.01, M. J. Frisch, G. W. Trucks, H. B. Schlegel, G. E. Scuseria, M. A. Robb, J. R. Cheeseman, G. Scalmani, V. Barone, B. Mennucci, G. A. Petersson, H. Nakatsuji, M. Caricato, X. Li, H. P. Hratchian, A. F. Izmaylov, J. Bloino, G. Zheng, J. L. Sonnenberg, M. Hada, M. Ehara, K. Toyota, R. Fukuda, J. Hasegawa, M. Ishida, T. Nakajima, Y. Honda, O. Kitao, H. Nakai, T. Vreven, J. A. Montgomery, Jr., J. E. Peralta, F. Ogliaro, M. Bearpark, J. J. Heyd, E. Brothers, K. N. Kudin, V. N. Staroverov, T. Keith, R. Kobayashi, J. Normand, K. Raghavachari, A. Rendell, J. C. Burant, S. S. Iyengar, J. Tomasi, M. Cossi, N. Rega, J. M. Millam, M. Klene, J. E. Knox, J. B. Cross, V. Bakken, C. Adamo, J. Jaramillo, R. Gomperts, R. E. Stratmann, O. Yazyev, A. J. Austin, R. Cammi, C. Pomelli, J. W. Ochterski, R. L. Martin, K. Morokuma, V. G. Zakrzewski, G. A. Voth, P. Salvador, J. J. Dannenberg, S. Dapprich, A. D. Daniels, O. Farkas, J. B. Foresman, J. V. Ortiz, J. Cioslowski, and D. J. Fox, Gaussian, Inc., Wallingford CT, 2013.
4. A. D. Becke, *J. Chem. Phys*., 1993, **98**, 5648–5652.
5. C. Lee, W. Yang, R. G. Parr, *Phys. Rev. B: Condens. Matter,* 1988, **37**, 785–789.
6. A. D. McLean, G. S. Chandler, *J. Chem. Phys.*, 1980, **72**, 5639–5648.
7. J. S. Binkley, J. A. Pople, W. J. Hehre, *J. Am. Chem. Soc.,* 1980, **102**, 939.
8. W. R. Browne, N. M. O'Boyle, J. J. McGarvey, J. G. Vos, *Chem. Soc. Rev.,* 2005, **34**, 641–663.
9. D. A. Zhurko, G. A. Zhurko, ChemCraft 1.5; Plimus: San Diego, CA. Available at http://www.chemcraftprog.com.